ETH
Eidgenössische Technische Hochschule Zürich
Swiss Federal Institute of Technology Zurich

TU Delft

pd | z Product Development Group Zurich
Produktentwicklungsgruppe Zürich

Master's thesis

Estimation of cardiac contractility, left-ventricular relaxation and cardiac output during rotary blood pump support

using the left-ventricular pressure

Author

Bob de Vries

Supervisor

Anastasios Petrou, PhD

Professor

Prof. Dr. Mirko Meboldt and Prof. Dr. ir. Michel Verhaegen

Nr.1249

Zurich, June 30, 2018

ETH
Eidgenössische Technische Hochschule Zürich
Swiss Federal Institute of Technology Zurich

TU Delft

pd|z Product Development Group Zurich
Produktentwicklungsgruppe Zürich

Master's thesis

Estimation of cardiac contractility, left-ventricular relaxation and cardiac output during rotary blood pump support

using the left-ventricular pressure

Dates

Start date 15.09.2017 End date 30.06.2018

Declaration of Originality

I hereby declare that I have written the present thesis independently and have not used other sources and aids than those stated in the bibliography.

_____

Bob de Vries

Confirmation

This thesis was written at and accepted by *pd*|**z** Product Development Group Zurich of ETH Zurich.

Supervisor

_____

Professor

_____

Acknowledgments

This document is a part of my Master of Science graduation thesis. The idea of doing my thesis on this subject came after I had my first encounter with the topic during my exchange semester at the University of Texas at Austin in the fall of 2016. The possibility to work in a project that may eventually help many people around the world gain a better quality of life was truly inspiring. I would like to thank my daily supervisor Anastasisos Petrou for his assistance during the writing of this thesis, his time and dedication and giving me a feeling of being welcome in the group. Furthermore, I want to thank my supervisors Professor Meboldt (ETH Zurich) and Professor Verhaegen (TU Delft) for the opportunity that they have given to me to conduct my thesis in such an amazing environment. Especially, I want to thank Professor Verhaegen for chairing the Board of examiners. Last, I would like to thank Dr. E. Steur and Dr. M. Kok for finding time to complete the Board of examiners and to grade my final Masters' examination.

Zürich, ETH, Federal Institute of Technology
June 30, 2018

Abstract

Objective: Estimators to accurately monitor ventricular relaxation, cardiac contractility and cardiac output (CO) during support of a left ventricular assist device (LVAD), based on the left ventricular pressure (LVP) and pump-intrinsic signals, were developed. The aim was to continuously monitor these cardiac parameters, hereby tracking the progression of disease and ensuring effectiveness of treatment.
Methods: Ventricular relaxation was estimated using the time constant of LVP decay, τ_p. Cardiac contractility was based on the maximum derivative of LVP, dP/dt_{max} versus the end-diastolic pressure (EDP). The CO was estimated using a hybrid monitoring scheme, that used the estimated pump flow (PF) in cardiac cycles with a closed aortic valve and a cardiovascular model in cycles with an open valve. The states of the cardiovascular model were estimated using an extended Kalman filter (EKF). The opening status of the aortic valve (AoV) was determined using a machine learning model that employed a quadratic discriminant analysis based on features of the LVP waveform. The estimators were evaluated using in-vitro and in vivo experiments on pigs that were earlier conducted within the Product Development Group Zurich ($\mathsf{pd}|\mathbf{z}$). The experiments contained preload, afterload, contractility and relaxation variations. The CO was evaluated in experiments from three control strategies (i.e. constant speed, physiological control and multi-objective control).
Results: The index τ_p uniformly resembled changes in left-ventricular relaxation. dP/dt_{max} versus EDP captured variations in cardiac contractility. Both were preload and afterload independent. The CO was estimated with a mean relative error of 11% compared to the true CO.
Conclusion: The feasibility and accuracy of using LVP based cardiac indices in LVAD assisted circulations was demonstrated.
Significance: The clinical implementation could provide clinicians with valuable and reliable information of the circulation of the patient, allowing for monitoring of progression of disease and improvement of treatment.

“Wherever you go, go with all your heart.”

--- *Confusius*

Contents

Glossary

List of Acronyms

AoV aortic valve

AoVF aortic valve flow

BTR bridge-to-recovery therapy

CVS cardiovascular system

DF II direct filter of type two

HMC hybrid mock circulation

PIP pump inlet pressure

RBP rotary blood pump

AHF acute heart failure

AoP aortic pressure

BTT bridge-to-transplant therapy

CO cardiac output

DT destination therapy

EDP end-diastolic pressure

EDPVR end-diastolic pressure volume relationship

EDV end diastolic volume

EKF extended Kalman filter

ESPVR end systolic pressure volume relationship

HF heart failure

HIL	hardware in the loop
HLM	heart lung machine
HR	heart rate
HRpEF	heart failure with preserved left ventricular ejection fraction
HRrEF	heart failure with reduced left ventricular ejection fraction
KF	Kalman filter
LPF	low-pass filter
LV	left ventricle
LVAD	left ventricular assist device
LVP	left ventricular pressure
LVV	left ventricular volume
MAE	mean absolute error
MCC	Matthews correlation coefficient
MCS	mechanical circulatory support
ML	machine learning
OG	outflow graft
P-V	pressure-volume
PF	pump flow
PI	proportional integral
PIP	pump inlet pressure
POP	pump outlet pressure
PS	pump speed
RMSE	root mean squared error
SP	systolic pressure
SV	stroke volume
SVR	systemic vascular resistance
VAD	ventricular assist device

List of Symbols

τ_1	Time-constant of exponential elastance during systole
τ_2	Time-constant of exponential elastance during diastole
τ_p	Time-constant of exponential left-ventricular pressure decay
d	Diameter of outflow graft
dP/dt_{max}	Maximum derivative of left ventricuar pressure
dP/dt_{min}	Minimum derivative of left-ventricular pressure
E_{lva}	Scaling parameter for the systolic part of the elastance
E_{lvb}	Parameter to control the baseline end-diastolic volume
e_{lv}	Left ventricular elastance
k_{sp}	Proportional systolic pressure controller gain
l	Length of outflow graft
$LVP(t)$	Left ventricular pressure
LVP_0	Left ventricular pressure whent diastole begins
LVP_∞	Left ventricular pressure asymptote $t \to \infty$
PS_{des}	Desired pump speed
PS_{ref}	Pump speed reference
SP_{ref}	Systolic pressure reference
t_τ	End-time of exponential elastance during diastole
t_{ee}	Time of end of ejection
v_{lv}	Left ventricular volume
R	Covariance of measurement noise

1 Introduction

1.1 Heart failure

Structural and/or functional anomalies of the heart can cause a clinical syndrome called heart failure (HF), resulting in a reduced CO and elevated pressures in the heart (Davis et al. (2015)). HF is a major cause of morbidity and mortality, having a great effect on patients and society. Approximately 2% of the adult population is affected. Incidence rises with age, with an affected population of 3-5% for those aged 65 years and older and even 10% among people over 70 years of age (Davis et al. (2015)). Before HF clinically manifests itself, patients can have asymptomatic structural and functional anomalies, such as systolic and diastolic dysfunction of the left ventricle (LV). HF can be subdivided into systolic and diastolic failure. Systolic failure is the loss in ability for the heart to contract normally, resulting in the heart not being able to push enough blood into the circulation. Diastolic failure is the loss of ability for the heart to relax during the resting period of the heart cycle. Systolic failure is commonly characterized as heart failure with reduced left ventricular ejection fraction (HRrEF). On the other hand, diastolic dysfunction, presents itself as heart failure with preserved left ventricular ejection fraction (HRpEF) and is caused by abnormalities in the filling capacity of the heart, such as LV hypertrophy and an enlarged left atrium (Van Riet et al. (2016)).

1.2 Treatment

Treatment of HF can mainly be subdivided into pharmacological treatment, non-surgical device treatment and mechanical circulatory support (MCS) and heart transplantation. The first two and last are beyond the scope of this thesis but are very well assessed by the ESC Guidelines for the diagnosis and treatment of acute and chronic HF (Ponikowski et al. (2016) and Davis et al. (2015)).

1.2.1 Mechanical circulatory support

Patients with chronic or acute HF who cannot sufficiently be treated with medical therapy, may benefit from MCS to unload the failing heart and thereby maintaining sufficient organ perfusion and stabilizing hemodynamics. Since the 1950s, pumps have been developed for MCS. Patients with acute heart failure (AHF) or cardiogenic shock can be treated with short-term MCS devices in a hospital setting. The use of these devices is usually limited to only a few days to weeks. After the patient is stabilized, it can be decided to install a device for long-term mechanical support, such as an LVAD.

1.3 Left Ventricular Assist Devices

An LVAD is a mechanical pump that supports the human circulation by extracting blood from the left-ventricle and afterwards pumping this blood into the ascending part of the aorta (Figure 2.1). LVADs that are being used clinically exist as either centrifugal or axial pumps. LVADs are currently used in three cases. As heart transplantation is not always possible for treatment of patients with end-stage HF, due to limited availability donors and the increase of patients with recurrent, chronic HF, LVADs are increasingly installed as an alternative to heart transplantation. Initially these devices where installed as a bridge-to-transplant therapy (BTT). However, due to technological advancements, nowadays they are being used for elongated treatment, ranging from months to years. Many patients receive an LVAD as destination therapy (DT) (Dunlay et al. (2016)). The survival rate among patients with long-term mechanical support is comparable to those with heart-transplantation (Riebandt et al. (2014)). Ongoing research focuses on using the LVAD for the third option, which is bridge-to-recovery therapy (BTR) therapy.

All current LVADs operate at a constant speed, which results in non-

physiologic flows in the human body. These non-physiologic flows are believed to lead to complications, which may eventually result in a number of severe adverse events, including stroke, gastro-intestinal bleeding and thromboembolism. The operation at constant speed is believed to lead to the adverse events as it can lead to over-pumping, resulting in LV suction and ultimately thrombosis, caused by damage of the LV. As opposed to over pumping, under pumping leads to congestion in the pulmonary circulation, ultimately resulting in right heart-failure. In order to detect the aforementioned complications and prevent adverse events from happening, multiple strategies can be used. The first is the development of physiologic control algorithms, as done by (Petrou et al. (2017)). The second possibility is accurate monitoring of the LVAD assisted circulation. Monitoring is important to track the progression of disease in LVAD patients as well as to detect and treat complications in an early stage. Furthermore, accurate monitoring can support physiologic control algorithms to obtain a better patient outcome.

Important properties of the circulation include the systolic properties of the heart, such as contractility. Besides the systolic properties of the heart, diastolic properties also play a vital role in determining the pumping ability of the heart. Diastolic heart failure accounts for about 50% of heart failure in patients with heart failure. Diastolic properties of the heart are measured during the relaxation phase of the heart-cycle and include measurements of filling, ventricular relaxation, stiffness and diastolic distensibility. (Paulus et al. (2007)). The measurement of these parameters often includes invasive or time-consuming procedures, such as echocardiography (Zile (2002), Kasner et al. (2007)).

Furthermore, the first generation of LVADs did not possess any sensors, hereby making real-time monitoring outside the hospital impossible. The second generation of LVADs were equipped with pump-flow estimators. Based on the pump-flow, many relevant monitoring indices have been developed, allowing for real-time low-level monitoring. Although, the availability of pump-flow estimators has been a large step forward for accurate monitoring, the indices based on pump-flow still have drawback such as preload and afterload dependency and the often-non-linear relation with the flow signal.

Moreover, developments of a new sensor technology, especially of a pump inlet pressure (PIP) sensor, have broadened possibilities of accurate monitoring. As the PIP sensor is able to directly measure the LVP, it is believed to be a valuable development to achieve better real-time monitoring in circulations that are supported by an LVAD.

1.4 Research goals

The goal of this theses is to explore the possibilities of this new sensor technology to develop monitoring algorithms that can be used to monitor in real-time. Hereto, three important cardiac parameters, 1) left-ventricular relaxation, 2) cardiac contractility and 3) cardiac output, were selected based on the literature survey that was conducted. The following goals were set for this thesis:

1. The implementation of a measure of left-ventricular relaxation and contractility into our testing environment and evaluation using simulation as well as in vivo data.
2. The estimation of the cardiac output making use of the pump-intrinsic signals and the left-ventricular pressure signal, for multiple control strategies.

To achieve the research goal, a dataset containing experiments from numerical simulations, in vitro data as well as in-vivo data will be used to analyze the performance of the selected indices. Chapter one will explain the experimental setup and our dataset in detail. Chapter two explains the methods that were used to derive and evaluate the selected monitoring indices. Chapter three presents the results, followed by a conclusion, discussion and recommendation for future research focus in the subsequent chapters.

2 Materials

2.1 The system

The models, signals and data that are used in this thesis all relate to the cardiovascular system of either humans or pigs that is supported by an LVAD with non-linear pump-characteristics. This means that the pressure to flow relation is non-linear in the operating range of the LVAD. The LVAD that is used has its inflow cannula inserted into the left-ventricle. The outflow cannula is connected to the aorta with an outflow graft. The pump-inlet pressure is measured at the inlet cannula of the LVAD. As the inflow cannula is directly inserted into the left-ventricle, the PIP and the LVP are interchangeable throughout this thesis. Furthermore, the pump outlet pressure (POP) is defined as the pressure at the outflow cannula of the LVAD. The aortic pressure (AoP) is the pressure at the end of the outflow graft at the insertion with the aortic arch. Last, the pump-intrinsic signals are defined as the pump speed (PS) and the motor current of the LVAD and are assumed to be measurable and thus known as is the case for all clinically implanted LVADs. Figure 2.1 shows an overview of the system.

2.2 Software and hardware

To develop and test the three selected monitoring indices, more specifically a measure of ventricular relaxation, ventricular contractility and the cardiac output, a broad environment was used. At the core of the development within our group of new algorithms, models and devices regarding the human heart, lies a verified numerical cardiovascular system model (Colacino et al. (2007)) that models the human circulation. Using this model allows for rapid and facile evaluation of such new developments. Based on this model a hybrid mock circulation (HMC) was developed by (Ochsner et al. (2013)), which combines the numerical cardiovascular system model and a physical rotary

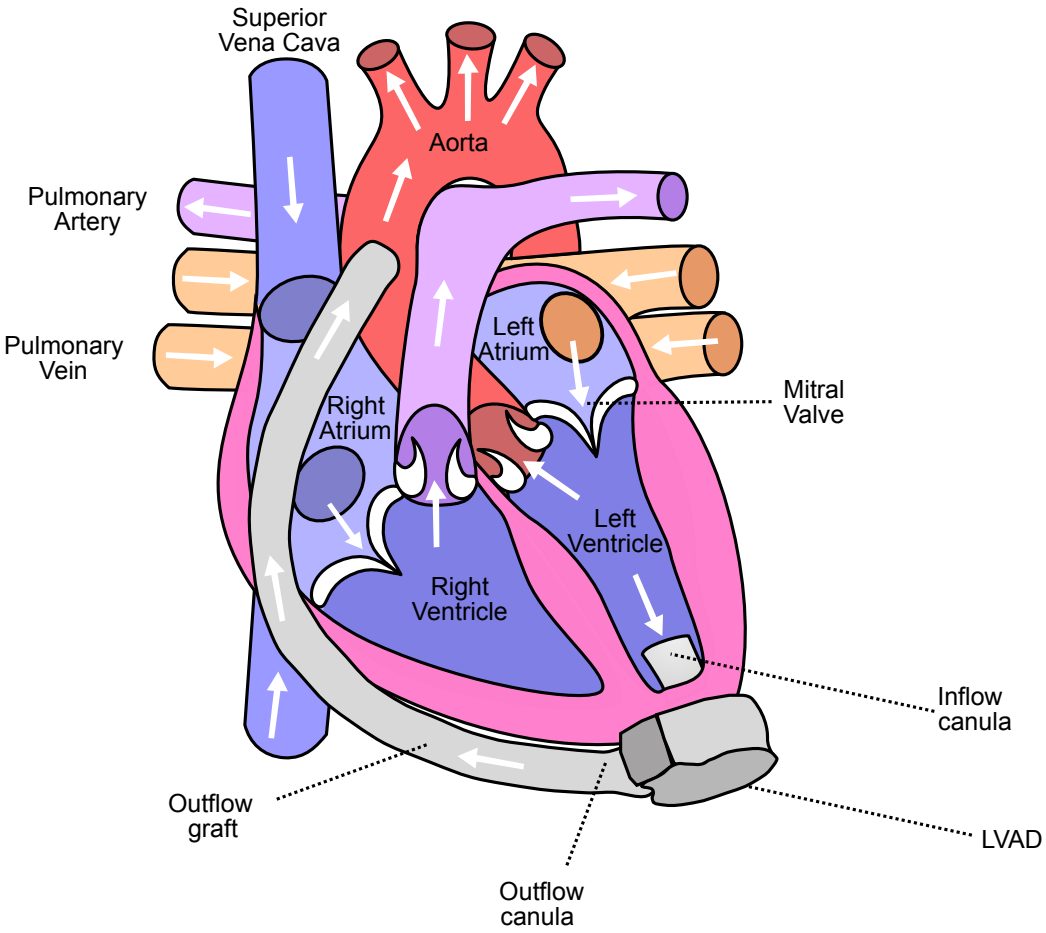

Figure 2.1: Schematic of the heart with an left ventricular assist device (LVAD).

blood pump (RBP) through a numerical-hydraulic interface, resembling the interaction of a simulated human with a real LVAD. Data obtained from experiments conducted on these environments were used for evaluation of the proposed algorithms in this thesis. As the similarity between either a numerical model or the HMC and a real human is limited, also in vivo data from acute animal trials with eight healthy pigs, that were previously conducted within in our group by (Ochsner et al. (2017)), was used for evaluation.

The test environments allowed for different modes of controlling the pump-speed of the LVAD, allowing for multiple levels of adaptation to hemodynamic changes and predefined objectives. The control strategies were a constant pump-speed, which is similar to all clinically used LVADs, and more sophisticated methods, namely physiological control and multi-objective control as proposed by (Petrou et al. (2017)), all of which are further explained in this

chapter. The data obtained using the numerical cardiovascular system model were solely gathered using a constant pump-speed. The data from the HMC contains experiments using all three control strategies. During the in-vivo experiments, both a constant pump-speed as well as a physiological controller were used. Using these three testing environments and different control modes, data was obtained from multiple experiments, including ones that mimicked physiological conditions that can be observed in real patients. The in sillico, in vitro and in vivo datasets are described in detail in this chapter. For each monitoring index a subset of the available data was collected for evaluation, described for each index individually. The collected data were then used to evaluate each of the three selected cardiac indices.

2.2.1 Cardiovascular model

For simulation of the interaction of a human and an LVAD, a complete mathematical model of the cardiovascular system was implemented in MATLAB/Simulink (The MathWorks, Inc., Natick, MA, USA). The very details of the model can be found in (Ochsner et al. (2013)). It comprises of the modeling of the cardiovascular system using electrical analogies of a closed-loop hydraulic system, together with a model of the LVAD that is used. The circuit consists of left- and right ventricles and atria, the systemic as well as the pulmonary circulation. The systemic and pulmonary arterial system are modeled using five-element Windkessel models, comprising of two capacitances, two resistances and one inductance. The pulmonary and systemic venous system is modeled with a classic Windkessel model, which consists of just one resistance and capacitance. The left and right ventricles were modeled using nonlinear time-varying elastances and internal resistances. Both the atria and ventricles contract following a time-varying elastance model. While evaluating the measure of ventricular relaxation this time-varying elastance model has been replaced by a function that exhibits mono-exponential pressure decay to allow for different levels of ventricular relaxation (Sun (1991)) . Furthermore, regulatory baroreflex mechanisms are implemented to auto-regulate the arterial systemic pressure, by means of the arterial systemic resistance. Also, the cardiac output CO is regulated by adapting the unstressed venous volume in the systemic venous circulation. Each subsystem of the numerical model is represented using lumped parameter models. The corresponding differential equations are solved using electrical analogies of the hydraulic components. (Colacino et al. (2007)). This model has been extended to emulate ventricular suction as well as to accurately mimic different viscosities of blood. A schematic containing the most important components of the model is depicted in Figure 2.2. The parameter values for the model that were used in this thesis correspond to the values that were used by Colacino

et al. (Colacino et al. (2007)).

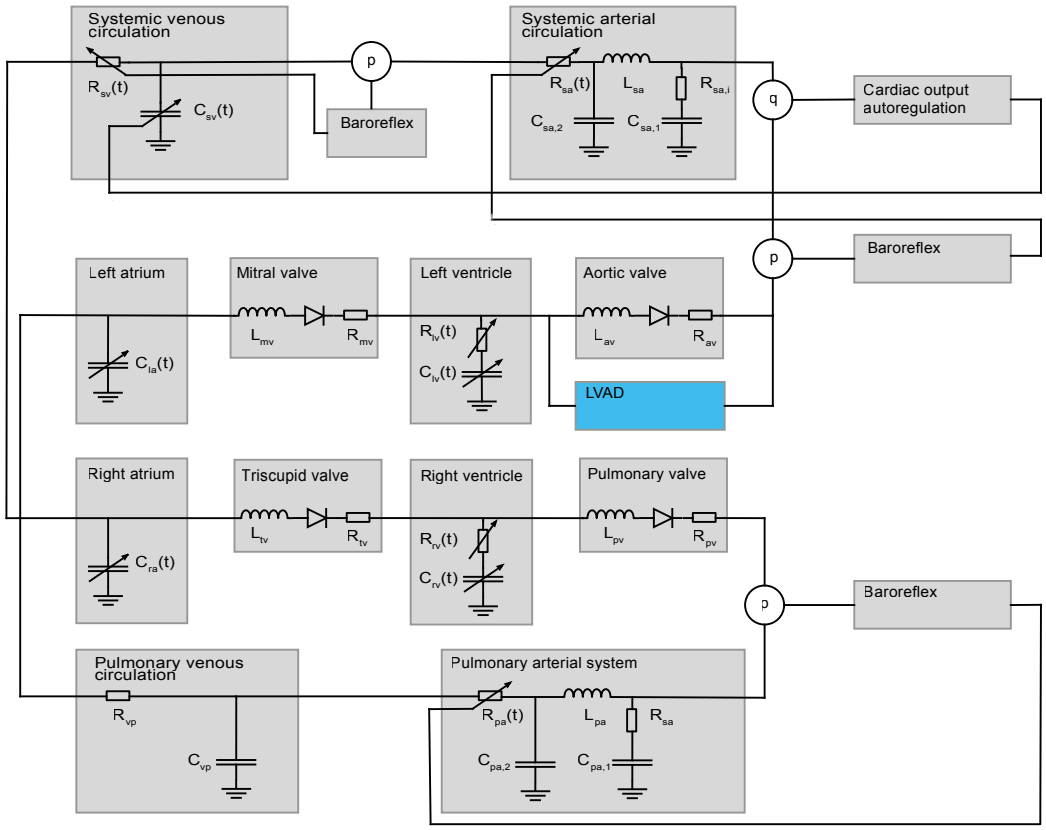

Figure 2.2: Schematic of the cardiovascular model as developed by Colacino et al. (Colacino et al. (2007)). The left ventricular assist device (LVAD) is highlighted in blue. The letter L represents an inductance, R a resistance and C a capacitance. The subscript to each of these letters correspond to the respective part of the circulation.

2.2.2 Hybrid Mock Circulation

To integrate a real LVAD into the evaluation process of the selected monitoring indices, all in vitro experiments were carried out on a HMC that was earlier developed in our group and described in detail by Ochsner et al. (Ochsner et al. (2013)). The HMC was developed based on the hardware in the loop (HIL) concept. The HMC consists of three parts, the validated numerical model of the human circulation (Colacino et al. (2007)), as described in previous section, an LVAD and a numerical-hydraulic interface. The hydraulic interface consists of two pressure-controlled fluid reservoirs, mimicking the left ventricle and aorta, and a flow probe. The HMC works as

follows; The flow through the LVAD is measured with a flow probe. The numerical model of the human circulation then calculates the left-ventricular and aortic pressures, which are subsequently applied to the reservoirs through a pneumatic interface. The adjustment of the pressures in the reservoirs results in a flow change through the LVAD after which a new loop of calculations begins.

The fluid-level in the reservoirs is kept constant by a back-flow pump that is controlled with a proportional integral (PI) controller with anti-reset-windup and roll off. Furthermore, the pressures generated by the numerical cardiovascular system model are tracked and controlled by two separate PI controllers with a lead extension. These controllers are extended with anti-reset windup to empty an over-full integrator and gain scheduling for different levels of fluid in the reservoirs. The parameters of these controllers were optimized by minimizing the complementary sensitivity function (Ochsner et al. (2013)). The use of an HMC allows for quick real-time in vitro simulation of different LVADs, control algorithms and patient characteristics. The HMC is shown in Figure 2.3.

For this thesis, instead of a clinically used LVAD, a non-implantable model of a mixed-flow turbodynamic blood pump, the Deltastream DP2 (Xenios AG, Heilbronn, Germany) was used, which is employed in the clinical setting for extra-corporeal circulatory life support or extra-corporeal membrane oxygenation. This pump has been modified to allow for controlling pump-speed as desired. This is in contrast with commercially implanted LVADs for which manufacturers do often not allow full access. For conducting our experiments, the HMC was run until steady state was reached.

2.3 Control strategies

The experiments for this thesis were carried out making use of three strategies to control the pump-speed of the LVAD. In the first control mode the LVAD is operated at a constant speed. To achieve this the speed of the rotor is kept equal to a pre-defined reference value throughout the operation of the LVAD, which is similar to the strategy that is used in all currently clinically implanted LVADs and thus is not adaptive to changing hemodynamics and circumstances.

The second is a preload based physiologic controller that aims to make the circulation behave in a physiological way and is implemented using a systolic pressure (SP) controller as proposed by Petrou et al. (Petrou et al. (2016)). The controller uses the measured SP at the pump-inlet of the LVAD as an

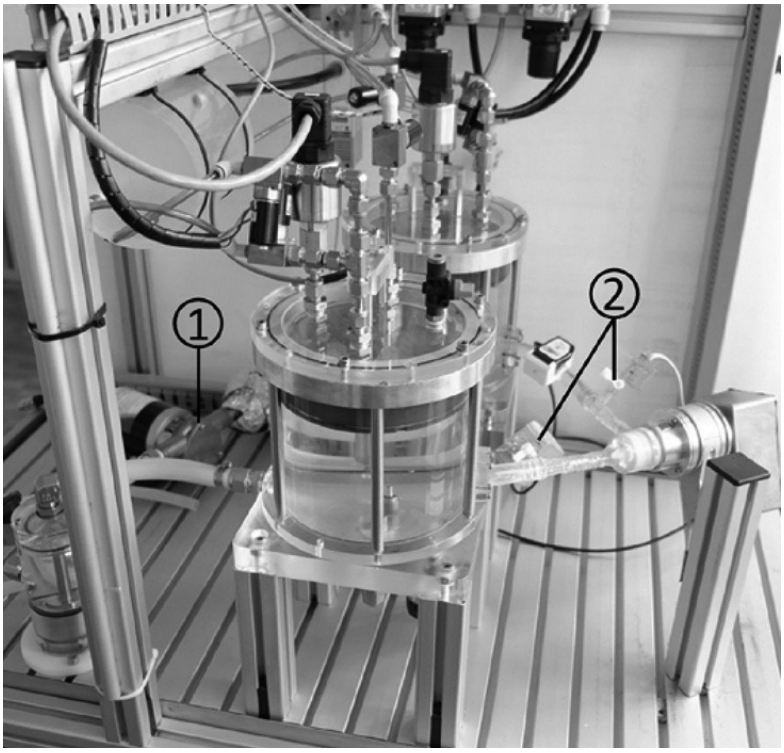

Figure 2.3: Picture of the hybrid mock circulation (HMC). The principle of operation and its components were published by Ochsner et al. (Ochsner et al. (2014)). The back-flow pump (1) has been replaced by a flexible impeller pump (Jabsco 18660 Series, Xylem Inc., NY, USA), and pump inlet and outlet disposable pressure transducers (2) (TruWave, Edwards, Life sciences, Irvine, CA, USA) were added.
Note. the above figure was reprinted with permission from Petrou et al. (Petrou et al. (2017))

estimate of the preload condition of the left-ventricle. The SP-controller is implemented as follows:

$$PS_{des} = k_{sp}(SP - SP_{ref}) + N_{ref} \tag{2.1}$$

where PS_{des} is the desired pump-speed (rpm), k_{sp} is the proportional gain, SP_{ref} is the SP at calibration. To calibrate the controller, first the constant pump-speed that yielded a desired CO was identified manually. The PS_{ref} and SP_{ref} were then saved at the desired operating point. k_{sp} was identified using a loop-shaping method with data from in-vitro experiments.

The multi-objective controller is described in detail in (Petrou et al. (2017)). The full control scheme uses the PIP and the pump-intrinsic signals, which

are PS and PF. The output is the desired pump-speed, PS_{des}. The system can be divided into three parts, 1) signal processing, 2) estimators and 3) controllers. The main part of the system is the PF adaptation controller, which is supplemented with an AoV opening controller, three different safety controllers and a speed amplitude controller to achieve pulsatility.

2.4 Experimental setup

For evaluation of the models and algorithms in this thesis, data from numerical simulations that were performed using the numerical cardiovascular system model could be used. Furthermore, in-vitro experiments on the HMC as described in previous section as well as in vivo experiments in eight healthy pigs was accessible. The experiments that were used for the evaluation of the monitoring indices were designed to simulate daily situations, such as exercise or an increased arterial blood pressure. The complete data sets of which experiments could be used are described in this section. For evaluation of each of the three selected monitoring indices a different subset of this data was used, described for the respective monitoring index individually.

Table 2.1: Varied parameters in the in sillico experiments of our study. All other parameters of the circulation remained fixed and were equal for each experiment

Exp	Description	Time (s)	HR (bpm)	UVV (mL)	SVR ($mmHg \cdot s/mL$)	PS (rpm)	Contractility (%)
1	Rest	[0, 60]	75	2520	1.11	4180	34
2	Preload variation	[0, 30, 35, 60]	75	[2520, 2520, 2020, 2020]	1.11	4180	34
3	Afterload variation	[0, 30, 35, 60]	75	2520	[1.11, 1.11, 1.51, 1.51]	4180	34
4	Contractility variation	[0, 30, 35, 60]	75	2520	1.11	4180	[10, 10, 20, 20]
5	Contractility variation	[0, 30, 35, 60]	75	2520	1.11	4180	[20, 20, 30, 30]
6	Contractility variation	[0, 30, 35, 60]	75	2520	1.11	4180	[30, 30, 40, 40]
7	Contractility variation	[0, 30, 35, 60]	75	2520	1.11	4180	[40, 40, 50, 50]
8	speed-ramp	[0, 30, 35, 60, 65, 90, 95, 120, 125, 150, 155, 180]	75	2520	1.11	[3250, 3250, 3500, 3500, 3750, 3750, 4000, 4000, 4250, 4250, 4500, 4500]	34

HR heart rate, UVV unstressed venous volume, SVR systemic vascular resistance, PS pump-speed
Note. experiments 1-3 were similar to Petrou et al. (Petrou et al. (2017) and Petrou et al. (2018))

2.4.1 Numerical simulation - in sillico

Experiments could be obtained from numerical simulations using the cardiovascular system model in combination with a validated model of the LVAD of interest, which is in our case the Deltastream DP2 (Xenios AG, Heilbronn, Germany). The range of experiments that can be carried out is infinite. For instance, an afterload variation could be applied to the system by changing the value of a single parameter, in our case the systemic arterial resistance, which conforms to an increase in arterial blood pressure. It is also possible to simulate the influence of more complex situations, such as an experiment that mimics exercise. In this case the heart rate (HR), unstressed venous volume, pulmonary vascular resistance, systemic vascular resistance as well as cardiac contractility are altered all at once. The experiments that were used for evaluation are depicted in Table 2.1. Experiment one is a rest experiment, without any induced variation. Experiment two is a preload increase, applied by a decrease in the unstressed venous volume. In experiment three the afterload on the heart is increased with an increase in the systemic vascular resistance. Experiment four, five, six and seven are a contractility increase of 10% with respect to a certain baseline contractility, defined at the beginning of the experiment. The last experiment is a gradual increase in pump-speed from 3250 rpm to 4500 rpm in steps of 250 rpm.

Table 2.2: Varied parameters in the experiments of our study. All other parameters of the circulation remained fixed and were equal for each experiment

Exp	Controller	Description	Time (s)	SVR (mmHg s/mL)	PVR (mmHg s/mL)	UVV (mL)	HR (bpm)	Contractility (%)
1	MOC, PC, CS	preload variation	[0, 20, 25, 80, 90, 120]	1.11	0.1	[2520, 2520, 2020, 2020, 3025, 3025]	80	34
2	MOC, PC, CS	Afterload variation	[0, 20, 25, 80, 90, 120]	[1.1, 1.1, 0.51, 0.51, 1.91, 1.91]	0.1	2520	80	34
3	MOC, PC, CS	Exercise	[0, 20, 30, 120]	[1.1, 1.1, 0.6, 0.6]	[0.1, 0.1, 0.05, 0.05]	[2520, 2520, 2220, 2220]	[80, 80, 100, 100]	[34, 34, 40, 40]
4	PC, CS	Contractility variation	[0, 20, 25, 80, 90, 120]	1.11	0.1	2520	80	[34, 34, 51, 51, 17, 17]
5	MOC, PC, CS	Sleep to wake	[0, 80, 100, 160]	[1.65, 1.65, 1.11, 1.11]	[0.09, 0.09, 0.076, 0.076]	[2300, 2300, 2485, 2485]	60	34
6	CS	Rest	[0, 160]	1.11	0.08	2500	90	34

SVR systemic vascular resistance, PVR pulmonary vascular resistance, UVV unstressed venous volume, HR heart rate, MOC multi-objective control, PC physiological control, CS constant speed
Note. Data from Petrou et. al (Petrou et al. (2017) and Petrou et al. (2018))

2.4.2 Hybrid mock circulation - in vitro

The dataset with in vitro data contained a total of fifteen experiments that were conducted on the HMC (Table A.1). The experiments can be subdivided into six groups of experiments, including a preload variation, an afterload variation, an exercise experiment, a sleep to wake experiment, a contractility variation and rest. All but the rest and sleep to wake experiments were carried out for all three different control strategies of the pump-speed, as described in previous section. However, the rest experiment was solely carried out for the constant pump-speed operation mode. The sleep to wake experiment was carried out for both physiological control as well as constant-speed, but not for multi-objective control. The experiments are summarized in Table 2.2. The experiments can be characterized by a variation of cardiovascular parameters at a certain moment in time. Real hemodynamic conditions were mimicked by varying either the systemic vascular resistance, pulmonary vascular resistance, unstressed venous volume, heart rate or contractility or a combination of these. For instance, an increase in blood pressure was achieved by increasing the afterload on the system by means of an increase in systemic vascular resistance.

2.4.3 Animal trials - in vivo

Besides simulation experiments using the numerical cardiovascular system model and HMC, in-vivo data was collected during acute animal trials with eight healthy pigs (m=91.13 ± 9.69kg) that were carried out by Ochsner et al. (Ochsner et al. (2017)). The LVAD that was used is the Deltastream DP2 similar to the one used in the HMC. Three different hemodynamic manipulations were applied, 1) a preload reduction, 2) a preload increase and 3) an afterload increase. The preload increase, and reduction were performed by either infusing or draining 500ml of blood with a heart lung machine (HLM). After each experiment, the hemodynamic state of the pig was brought back to its baseline. For example, after a preload reduction experiment 500ml of blood was infused back into the pig, before applying another hemodynamic change. The afterload was changed by inflating an occlusive balloon catheter that was inserted into the descending aorta. The experiments were carried using a constant pump-speed and physiologic control that used either the LVP or the left ventricular volume (LVV) as the preload condition of the heart. An in-depth description of controller calibration for each pig can be found in (Ochsner et al. (2017)). For this thesis, from the experiments with physiologic control only the pressure-based controller experiments were used.

Table 2.3: This table shows a summary of the experiments that were carried out during the in vivo experiments on eight healthy pigs.

Exp	Description	Variation	CS	PC
1	Preload increase	Infusion of 500ml blood	X	X
2	Preload reduction	Extraction of 500ml blood	X	X
3	Afterload increase	Inflation of occlusive balloon catheter	X	X
4	Speed ramp	Gradual increase of pump-speed	-	-
5	Rest	None	X	-

CS constant speed, PC physiological control

Furthermore, a so-called speed-ramp experiment was performed at different stages during the experiments. During speed-ramp experiments the pump-speed is gradually increased, which makes it possible to record the pressure-volume (P-V) loops at different operating points of the heart. From these P-V loops, important information, such as the end-diastolic pressure volume relationship (EDPVR), as well as the end systolic pressure volume relationship (ESPVR) can be derived. A summary of the conducted experiments is depicted in Table 2.3. Experiments 1-3 were conducted for all control strategies of the pump-speed. For the speed ramp experiment, the pump-speed was not controlled using either control strategy. The rest experiment was carried using constant pump-speed only, without any induced variation.

3 Methods

This chapter describes the derivation of the three selected monitoring indices in detail as well as the approach that was followed to evaluate their performance. Estimation of left-ventricular relaxation was based on determination of τ_p, a measure of LVP decay. Monitoring contractility relies on the computation of the maximum derivative of LVP, dP/dt_{max}, with an adjustment to the EDP. The cardiac output is estimated using a hybrid monitoring scheme that combines multiple signals, estimators and models. The indices for ventricular relaxation and cardiac contractility solely make use of the pump-inlet pressure signal. The estimation of the CO requires a more complex scheme that makes use of both the pump-inlet pressure signal as well as the pump-intrinsic signals (i.e. motor-current and pump-speed). The full monitoring scheme is explained in detail in this chapter. Furthermore, the subset of the experiments that were used for evaluation of each index from either numerical simulations, the HMC or in vivo experiments is presented for each index individually.

3.1 Ventricular relaxation

Ventricular relaxation conforms to the ability of the heart to expand during the diastole of the heart cycle. Relaxation properties can be influenced by physical properties of the heart, such as a stiffened ventricular wall. The accurate tracking of ventricular relaxation can therefore possibly give insights in the progression of physical diastolic properties of the heart.

3.1.1 Model

As shown by Weiss et al. (Weiss et al. (1976)) the waveform of the LVP during diastole follows an exponential decay in unassisted hearts. Therefore, inspired by Weiss et al., this method was extrapolated to the case in which the circulation is assisted by an LVAD. To capture changes in relaxation

Table 3.1: This table shows the nominal parameters for the bi-exponential elastance function

Parameter	Value
E_{lvb}	0.05
E_{lva}	3
$e_{lv}\|t_{ee}$	calculated during simulation
τ_1	0.3
t_{ee}	0.4165
t_τ	0.833
τ_2	[0.024, 0.034, 0.043, 0.051, 0.06, 0.063] (defined by user)

properties, an exponential curve is fitted to the diastolic part of the LVP signal. The time-constant, τ_p, of this exponential function is then calculated, which has been shown to be correlated with ventricular relaxation in both healthy and diseased hearts in an unassisted circulation. Therefore, the current elastance model of the left ventricle was replaced with a bi-exponential function (Sun (1991)). The elastance is defined as the change in pressure divided by a change in volume. The implementation of this elastance function leads to a mono-exponential decay of the LVP waveform during diastole in our simulation environment and allows for adjusting a parameter closely related to the time constant of LVP decay (Moscato et al. (2012)). The left-ventricular elastance is modeled using the following equation:

$$e_{lv} = \begin{cases} E_{lva}(1 - e^{\frac{-t}{\tau_1}}) + E_{lvb} & 0 \leq t < t_{ee} \\ (e_{lv}|t_{ee} - E_{lvb})e^{\frac{-(t-t_{ee})}{\tau_2}} + E_{lvb} & t_{ee} \leq t < t_\tau \end{cases} \tag{3.1}$$

where the LVP is defined as e_{lv}, the elastance, times the change in v_{lv}, the LVV. E_{lvb} controls the baseline end diastolic volume (EDV), E_{lva} is a scaling parameter for the systolic part of the elastance. $e_{lv}|t_{ee}$ is the maximum elastance of the left ventricle, which is the left ventricular elastance, $e_l v$, at the end of ejection t_{ee}. τ_1 and τ_2 are the time-constants of the rising and decaying part of the left-ventricular elastance respectively. Table 3.1 represent the nominal parameter values as used in our experiments. The first three parameters were identified for a human heart by Sun et al. (Sun (1991)). t_{ee} and t_τ were adjusted to comply with the cardiovascular system model that was use.

The exponential function that was fitted to the decaying part of the LVP signal to determine τ_p, is represented in Equation 3.2 (Moscato et al. (2012)).

$$LVP(t) = (LVP_0 - LVP_\infty) \cdot e^{-\frac{t}{\tau_p}} + LVP_\infty \tag{3.2}$$

Here $LVP(t)$ is the left ventricular pressure, LVP_0 is the pressure at time $t = 0$, when diastole and thus ventricular relaxation starts. LVP_0 equals the $t = t_{min}$, for which the time derivative of LVP (dP/dt_{min}) is minimal. LVP_∞ is the pressure asymptote for $t \to \infty$ and τ_p is the time constant of LVP decrease that is to be determined.

3.1.2 Experiments

In sillico

The evaluation of τ_p was performed using simulations for six relaxation conditions. The values of the rate of ventricular elastance decay that were selected are: 24, 34, 43, 51, 60 and 68 milliseconds which covers the range of healthy and diseased hearts (Moscato et al. (2012)). These changes were induced by varying the parameter τ_2 in the model of the bi-exponential elastance, described in previous subsection in Equation 3.2.

Pre- and afterload changes were simulated by changing the unstressed venous volume from 2520 to 2020 ml and the systemic arterial resistance from 1.11 to 1.51 $mmHg \cdot s/ml$ respectively in separate experiments, as can be seen in Table 2.1 experiment two and three. For these experiments, pump-speed was kept constant at 4180 rpm and the HR at 75 bpm.

The influence of pump-speed on τ_p was assessed by increasing the pump-speed from 3250 to 4500 rpm, with an interval of 250 rpm, for all selected values of ventricular elastance decay, Table 2.1 experiment five. Experiments that exhibited ventricular suction were not included.

In vivo

The validity of τ_p in real animals has not yet been established. Therefore, in order to evaluate the performance of τ_p, data of speed-ramp experiments (i.e. the pump-speed is slightly increased slowly over time) was taken together with subsequent experiments with a constant pump-speed that were carried out during the acute animal trials.

By using data of speed-ramp experiments, the EDPVR was derived. The EDPVR is commonly regarded as containing information about the relaxation

properties of the heart. The aim was to acquire the relaxation state of the heart by obtaining the EDPVR at several instances in time. A different EDPVR was assumed to conform to a different relaxation state of the heart. In our data set speed-ramp experiments were followed by experiments with a constant pump-speed. τ_p was obtained from these constant pump-speed experiments. The EDPVR in the speed-ramp experiments was assumed to represent the actual relaxation state of the heart at a certain time instance and was used as control for τ_p, as calculated in a constant speed experiment following a respective speed-ramp experiment. Experiments that did not have accurate LVP or LVV measurements, or no such measurements at all, were excluded. Also, if in between a speed-ramp experiment and the following constant-speed experiment, the hemodynamic state of the pig was knowingly altered (i.e. by inducing volume or the administering of drugs) from the baseline state, the respective experiments were excluded. This led to a total of twenty speed-ramp and twenty constant-speed experiments derived from data from five different healthy pigs. The performance was determined by visually observing a trend in direction and magnitude of the EDPVR and corresponding value for τ_p.

3.2 Contractility

3.2.1 Model

To determine contractility, the relation dP/dt_{max} versus EDP was used, which is the maximum derivative of LVP during systole, versus the EDP respectively, as it has been shown to be a promising and reliant index of contractility and to be relatively independent from pre- and afterload changes in experiments in canine hearts (Mason et al. (1971)). This method consists of two phases; In the first phase dP/dt_{max} is calculated for each beat in a respective experiment. Afterwards, the EDP is calculated by determining the pressure value in the right lower corner of the P-V loop of each separate heart-beat. Hereto, the P-V loop is subdivided into four quadrants, where the quadrants are separated by the mean of the LVP and the LVV. In the right-lower quadrant, thus where the LVP is larger than the mean LVP and the LVV is smaller than the mean LVV, the EDP is determined by finding the maximum value of the LVP multiplied by the LVV. Figure 3.1 shows a schematic of a typical P-V loop. The blue lines divide the P-V loop into four quadrants, such that the EDP can be found in the lower-right quadrant. Furthermore, the ESPVR and EDPVR are highlighted.

3.2.2 Experiments

In sillico

To test the validity of dP/dt_{max} versus the EDP as a valid pre- and afterload dependent index of contractility, three experiments were performed for different starting values of contractility, 10%, 20%, 30% and 40% compared to a healthy heart, thus ranging from a very diseased to diseased heart. The first experiment was an increase of the preload, by decreasing the unstressed venous volume from 2520 to 2020 ml. The second experiment was an afterload increase, achieved by an increase in the systemic vascular resistance (SVR) from 1.11 to 1.51 $mmHg \cdot s/mL$. These two experiments were used as control experiments for the third experiment, in which contractility was changed by 10%, starting from the four starting values of contractility. The experiments are summarized in Table 2.1, experiments two, three and four. In this way the individual influence of the respective hemodynamic changes on dP/dt_{max} versus EDP, could be evaluated. The effects of the hemodynamic changes were visually inspected.

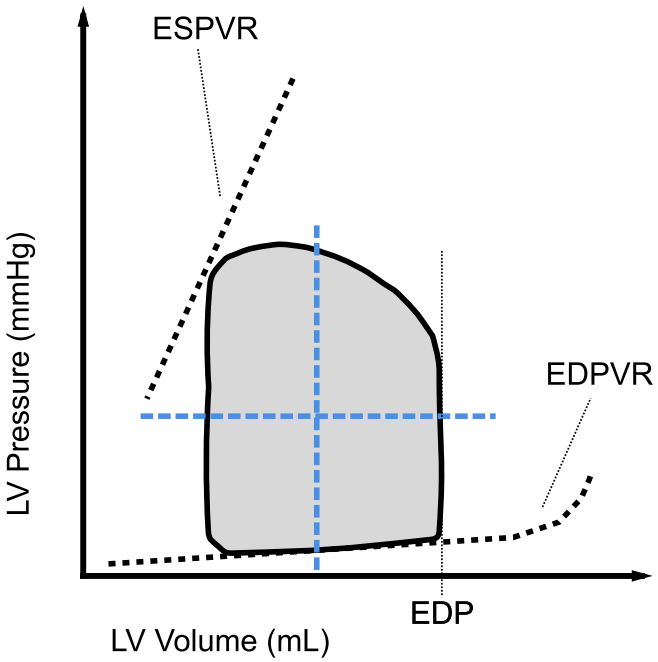

Figure 3.1: Schematic of a pressure-volume (P-V) loop, divided into four quadrants. The (end systolic pressure volume relationship (ESPVR), end-diastolic pressure volume relationship (EDPVR)) and end-diastolic pressure (EDP) are highlighted.

In vivo

For evaluation dP/dt_{max} versus EDP in vivo, data is required from experiments in which the contractile state of the heart changes, leaving all other factors equal. Although, no experiments were performed with the specific goal of collecting such data in our group, two experiments were available in which adrenaline was infused to two separate animals, albeit for other reasons such as to keep them alive during surgery. During these two experiments, the contractile state of the heart is assumed to be changed by adrenaline infusion leaving all other parameters, such as pump-speed and blood volume constant. dP/dt_{max} versus EDP was calculated just before and after the adrenaline infusion. The change in dP/dt_{max} versus EDP was visually observed to determine a correlation between the respective measure and the contractility change due to the adrenaline infusion.

3.3 Cardiac Output

The cardiac output describes the amount of blood that is being pumped by the heart per unit time and is defined as stroke volume stroke volume (SV) times HR, usually in liters per minute. In the case a circulation is supported by an LVAD, the CO somewhat loses its meaning as two separate mechanisms, and not solely the heart, contribute to the amount of blood that is being pumped into the aortic arch. Therefore, in the assisted case, the combined flow that is generated by the LVAD as well as the remaining heart function as measured in the aortic arch is used as a measure of CO.

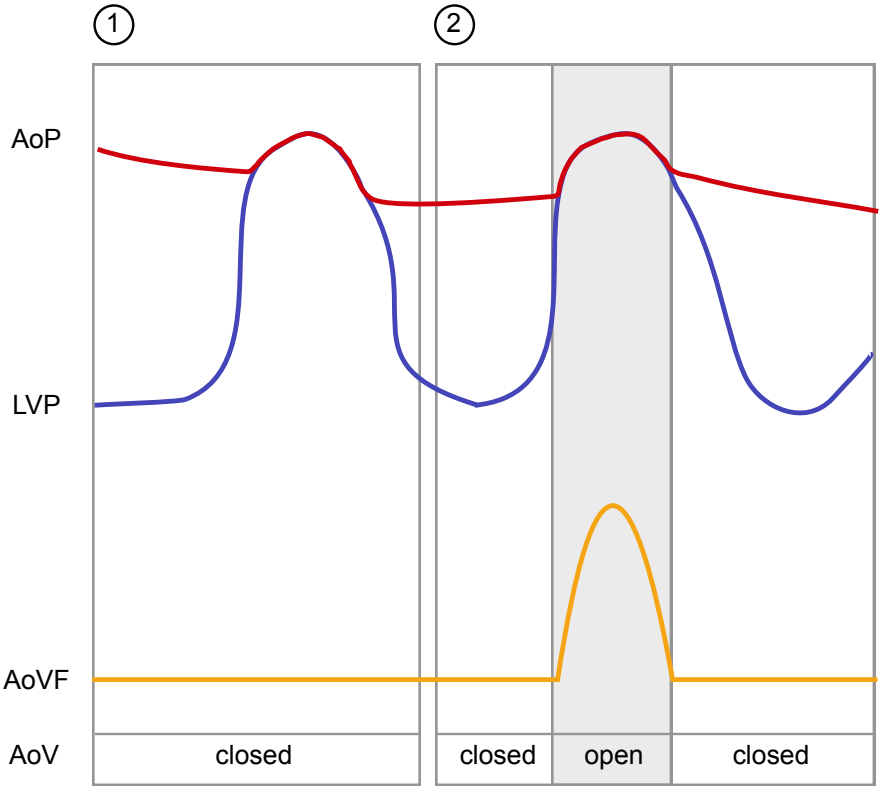

Figure 3.2: Important signals for two heart cycles with a closed (1) and open AoV (2). The aortic pressure (AoP) is depicted in red, the left ventricular pressure (LVP) in blue and the aortic valve flow (AoVF) in yellow. Also, the status of the aortic valve (AoV) is given.

Figure 3.2 shows a schematic of two heart cycles which are existent in patients with LVAD support. During the first heart cycle the AoV does not open,

hence no positive AoV flow occurs, which means that the complete CO is determined by the PF through the LVAD. However, for the second heart cycle, the AoV does open, which results in a positive flow through the AoV. Although, for both cycles the waveform of the LVP seems almost identical, it is known that slight differences exist between the distribution of the LVP in the two cases. The monitoring scheme that was developed, first uses a machine learning (ML) model to capture this difference in distribution and predict the opening of the AoV within a cycle. Based on the prediction of the ML model, the CO is then either determined by an estimation of the PF through the LVAD, or by estimation using a combination of simplified cardiovascular model, a Kalman filter (KF) and an EKF.

In case the circulation is under full-support, which means that the AoV stays closed during a complete heart cycle, the CO is equal to PF through the LVAD. However, in case the AoV opens during a heart cycle and the system is under partial-support, a combined flow generated by the heart as well as the LVAD result in the CO. Therefore, a hybrid model is used, where the selected model is based on the opening status of the AoV. For each heart cycle, the monitoring scheme is initiated with an estimation of the opening status of the AoV, making use of a ML model. Afterwards, either a simple model of the flow through the LVAD is used for determining the CO in the full-support case. For cycles that contain an opening of the AoV, the period of opening within such a cycle is estimated based on the PIP. During the closed part of the heart cycle, the CO is estimated using the PF estimator. However, for the time that the AoV is opened the CO is estimated using a simplified version of the cardiovascular system as described in previous chapter. The states of this model are estimated using an EKF as the system is non-linear. In parallel a KF is employed to keep the states and covariance matrix consistent throughout the estimation during the closed part of the heart cycle where the system is considered linear. The cardiovascular model uses the estimated PF and the measured LVP, which is equal to the pump-inlet pressure, as inputs. The output of the model, the aortic pressure, is then compared with the aortic pressure estimation that is derived through a hydraulic model. Subsequently, the error is used to update the states and to arrive at an estimation of the CO.

Figure 3.3 shows a schematic overview of the monitoring scheme that was used to determine the CO in this thesis. The scheme can be subdivided into three main parts, 1) pre-processing of data, 2) cardiac output estimation and 3) after-processing. The main subsystems are enumerated (block S1 - S6). To monitoring scheme was developed based on the pump-intrinsic signals and PIP and is in detail described in this section. First, the PIP and pump-intrinsic signals that are used as inputs to the monitoring scheme are processed to filter noise and to extract the required features. Then

the PF estimator and aortic pressure estimator, are implemented. These estimators, together with the PIP are then used in the final CO estimation. The estimators are described in detail in the following subsections. The full scheme and individual components are evaluated based on a subset of experiments presented in the preceding paragraph and outlined in detail in this section.

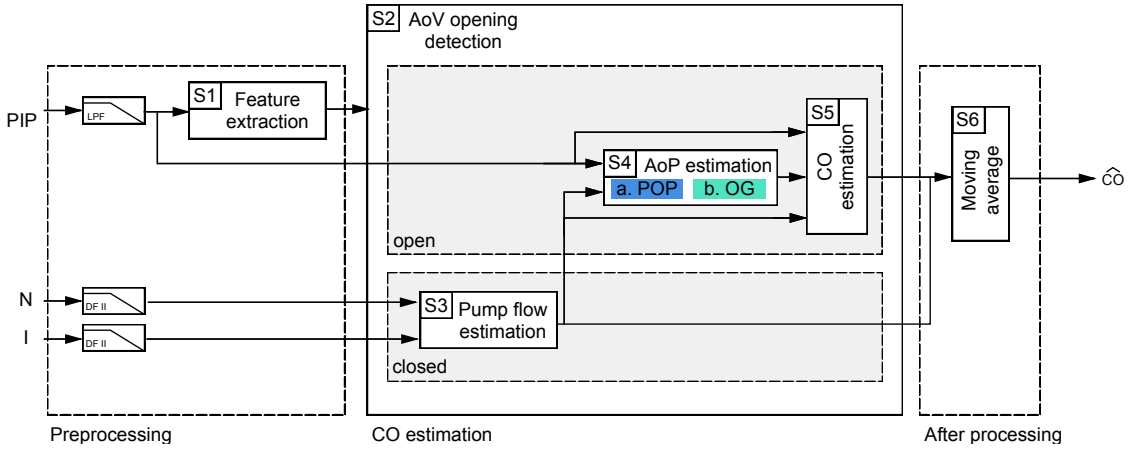

Figure 3.3: Overview of the monitoring scheme to estimate cardiac output (CO). The scheme makes use of the pump inlet pressure (PIP), N the pump-speed, I the motor-current, the aortic pressure (AoP), the pump outlet pressure (POP), the outflow graft (OG), aortic valve (AoV), a low-pass filter (LPF) and direct filter of type two (DF II).

3.3.1 Monitoring scheme

Preprocessing and feature extraction (S1)

The input signals to our model were processed to filter noise. In case of the PIP, the filtering was implemented using a first-order low-pass filter with a cut-off frequency of 25Hz. The pump-speed, N, and the motor-current, I, were filtered using Direct Form II discrete filters of which the parameters were identified in both static as well as dynamic experiments on the HMC.

After filtering, features that were needed were extracted (block S1 - Figure 3.3). The PIP was segmented into separate heart cycles by extracting the systolic pressure SP, which is the maximum pressure during systole, and EDP for every heartbeat. The HR was determined as the time between two consecutive systolic pressure values.

Furthermore, the time where a possible AoV opening takes place within a

heart-beat was extracted. It is solely possible for the AoV to open in between the occurrence of the end-diastolic pressure EDP and the SP. Based on the gradient of the PIP, the time close to a possible AoV opening, where the PIP equals the diastolic aortic pressure, was found. Hereto, the latest sample of PIP in between the interval of EDP and SP that is larger than a 30% of the maximum gradient of the PIP within that interval was obtained. As this range is extracted for every heart cycle, this method cannot distinguish cycles with or without an AoV opening. For this reason, the AoV opening is predicted using an AoV opening detector, which is described in the following section.

Aortic-valve opening detection (S2)

To predict the AoV opening status (block S2 - Figure 3.3), meaningful uncorrelated features were extracted from the distribution of the filtered PIP during the systolic phase of the heart cycle. The systolic phase of the heart cycle was defined as follows; For every heart cycle 40% of the systolic pressure value was extracted. Then on both sides of the systolic pressure, the values that were closest to 40% of the systolic pressure were found. The kurtosis, crest factor and skewness over the range between the previously found points were calculated using MATLAB built-in functions. These features were then used by the ML model that used a quadratic discriminant analysis to classify the opening status of the AoV by learning a mapping between the input feature space and the desired outputs (unpublished data in our group by M. Kanakis). The AoV opening detection uses the full systolic part of the corresponding heartbeat. Thus, the opening status of the AoV can solely be detected after a full beat has almost finished. Therefore, all signals to be used in the remaining part of the CO detection are delayed by one heart beat as determined by calculating the time between two consecutive systolic pressure values.

PF estimator (S3)

As the CO consists of either the PF alone or a combination of the PF and the AoV flow, a PF estimator was used to determine the PF. The PF estimator (block S3 - Figure 3.3) that was used, has originally been developed by Granneger et al. (Granegger et al. (2012) using a first-order dynamic model of a brush-less direct-current motor (BLDC). This model uses the pump current and pump-speed as its inputs. The estimator is described by equation 3.3.

$$J(\omega(t))\frac{d\omega(t)}{dt} = \tau(t) - a \cdot Q(t) \cdot \omega(t) - b \cdot \omega(t) - c \cdot \omega(t)^2 \qquad (3.3)$$

where $Q(t)$ is the pump flow and $J(\omega(t))$ is the dynamic coefficient. $\tau(t)$ represents the mechanical motor torque, $\omega(t)$ is the rotational speed and a, b and c are static coefficients. The coefficients have been identified using static and dynamic experiments on the HMC for a large range of experiments.

Aortic-pressure estimation (S4)

The AoP (block S4 - Figure 3.3) was estimated based on two different methods. If the AoV opened within a heart cycle, then a method proposed earlier by Petrou et al. (Petrou et al. (2017)) was used. This method assumes that the PIP approximates the AoP during systole. If the AoV stayed closed, the AoP was estimated using a model that describes the interaction between the LVAD and the circulation. The method is based on the differential equation of a turbo-dynamic LVAD (Granegger et al. (2012), Moscato et al. (2009)) and estimates the POP from the PIP, pump-speed and PF. By modeling the outflow graft that connects the pump outlet and the aorta, the AoP is estimated.

Pump-outlet pressure estimation (S4 - a) For a turbo-dynamic LVAD the change in the pump-outlet pressure (POP), is given by equation 3.4.

$$POP(t) = PIP(t) + a \cdot \omega(t)^2 - b \cdot Q(t)c \cdot Q(t) \cdot |Q(t)| - L\frac{dQ(t)}{dt} \qquad (3.4)$$

here, $Q(t)$ is the pump flow, $\omega(t)$ is the rotational speed, L is the fluid inertia, a is a parameter related to pump-speed and b and c are the linear and quadratic hydraulic resistances of the LVAD, respectively. Here a, b, c and L were identified as $5.81e^{-6}$, 0.70, 1.79 and 0.61 respectively for $Q(t)$ greater than zero. For $Q(t)$ smaller than zero b was $-4.32e^{-7}$ and c was 4.57. The derivative of the PF, $\frac{dQ(t)}{dt}$, was filtered using a lowpass filter with a cut-off frequency of 4000 Hz. The AoP equals the POP minus the pressure drop that occurs over the outflow-graft of the LVAD. The graft can be modeled accordingly.

Outflow graft (S4 - b) The outflow cannula of the LVAD is connected to the aorta using an outflow graft, which results in a pressure drop after the

LVAD. Therefore, the aortic pressure can be estimated by using the POP and correcting for a pressure drop over this outflow graft. The outflow graft as used on the HMC in our group, as well as for the in vivo experiments, has been modeled in our group as a perfect cylinder and its parameters have been identified using static and dynamic data collected on the HMC. The total pressure drop over the outflow graft can be modeled as the sum of three individual pressure losses due to 1) Darcy Weisbach loss, 2) pump-outlet loss and 3) a hydrodynamic loss (Equation 3.5).

$$\Delta_{DW} = \phi_1 \cdot \frac{l}{2d} \cdot \rho \cdot V \tag{3.5}$$

$$\Delta_{outlet} = \phi_2 \frac{\rho \cdot V^2}{2} \tag{3.6}$$

$$\Delta_{dynamic} = \frac{\rho \cdot V^2}{2} \tag{3.7}$$

combining the three individual pressure losses gives the total pressure loss:

$$\Delta_p = \Delta_{DW} + \Delta_{outlet} + \Delta_{dynamic} \tag{3.8}$$

here l= 0.2m and d= 0.0127m are the length and diameter of the outflow graft respectively. V is $\frac{Q(t)}{a}$, where $Q(t)$ is the flow in cubic meters and $a = \frac{\pi \cdot d^2}{4}$ the area of the cross section of the outflow graft. ρ was identified as 1080 $\frac{kg}{m^3}$, $\phi_1 = 0.04$and $\phi_2 = 0.66$ using static and dynamic experiments on the HMC.

Cardiac output estimation (S5)

The CO estimator (block S5 - Figure 3.3) works differently for either a closed or open AoV as determined by the AoV status estimator. Each of the two cases is described in this section.

Closed aortic valve In case the AoV has been determined to stay closed during a heart cycle, the cardiac output is solely generated by the flow through the LVAD. Therefore, the output of the PF estimator (block S3 - Figure 3.3) is used to determine the flow in the aortic arch. A moving average filter, that averages the PF estimate over each heart cycle, is applied to the estimated flow, resulting in an estimate for the CO.

Open aortic valve However, if the AoV has been predicted to have opened, the heart cycle can be divided into two parts, 1) the part where the AoV is closed and 2), the part where the AoV is opened. For the part of the heart cycle where the AoV is closed, the PF estimator (block S3 - Figure 3.3) is used to determine the flow in the aortic arch. However, for the part where the AoV is opened, an EKF is used to estimate the states of a simple non-linear cardiovascular system model (Rüschen et al. (2017)). In order to assure the consistency of states and the covariance matrix throughout the filtering process, a KF is used when the AoV is closed and the system is linear.

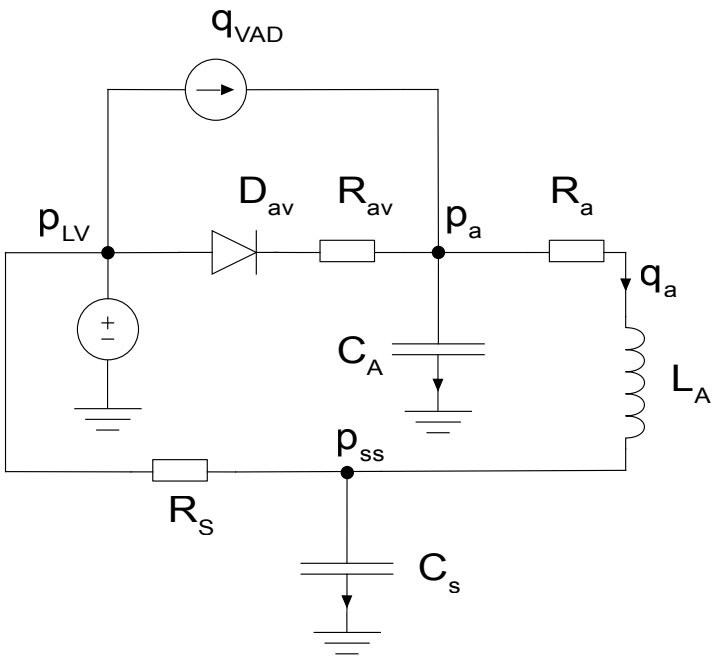

Figure 3.4: Simplified cardiovascular model as proposed by Rüschen et al. (Rüschen et al. (2017)). Here q represents flow, p represents pressure, C is a capacitance, R a resistance, L an inductor and D a diode. The subscripts lv, av, a, ss and vad represents the left-ventricle, the AoV, the systemic circulation and the ventricular assist device respectively.

The cardiovascular system (CVS) model that is being used for CO estimation is a simplification of the model as described by Simaan et al. (Simaan et al. (2009)) The one that was used solely contains elements that have an important effect on the dynamics of the aortic arch as proposed by Rüschen et al. (Rüschen et al. (2015)) and depicted in Figure 3.4. Here the CVS is modeled using electrical analogies. Due to the PIP sensor that measures LV pressure, the hydraulic properties of the left ventricle can be neglected. The left ventricle is modeled as a voltage source, where voltage is the electrical

Table 3.2: Nominal parameter values for the cardiovascular system model of a human

Parameter	Value	Unit
R_{av}	0.00375	$mmHg \cdot s \cdot mL^{-1}$
C_a	0.9	$mL \cdot mmHg^{-1}$
R_a	0.1	$mmHg \cdot s \cdot mL^{-1}$
L_a	0.0003	$mmHg \cdot s^2 \cdot mL^{-1}$
C_s	85	$mL \cdot mmHg^{-1}$
R_s	1.11	$mmHg \cdot s \cdot mL^{-1}$

analogy of pressure. Furthermore, the ventricular assist device (VAD) is modeled as a current source, an analogy of flow. The AoV is modeled using a resistance, R_{av} and a diode, D_{av}, implicating blood can only flow in one direction. Moreover, the aortic arch is modeled with a resistance, R_a and a compliance, C_a. The systemic circulation consists of a resistance, R_s and a compliance, C_s. Last, the inertance of blood is modeled using a single inductor, L_a. The nominal parameters of each of these six variables for a human can be found in Table 3.2. The parameter values were deducted from the full cardiovascular system model as described in previous chapter. The right ventricle, atria and pulmonary circulation of the heart are unmodeled as it is considered of little influence in the estimation of CO.

This cardiovascular model can be described using a lumped parameter state-space representation, where the aortic pressure p_a, the aortic flow rate q_a and the system pressure p_{ss} are the states of the system. The inputs to this system are the LVP,p_{lv}, and the flow through the LVAD, q_{vad} as these are the active elements. The output of the system is taken as the only state that can be derived using the aortic-pressure estimate (Section 3.3.1).

The state-vector is given as:

$$x = \begin{bmatrix} p_a & q_a & p_{ss} \end{bmatrix}^T \text{ and the input vector } u = \begin{bmatrix} p_{lv} & q_{vad} \end{bmatrix}^T \tag{3.9}$$

Which leads to the following state-space representation (Equation 3.10):

$$\begin{bmatrix} \dot{p}_a \\ \dot{q}_a \\ \dot{p}_{ss} \end{bmatrix} = A \begin{bmatrix} p_a \\ q_a \\ p_{ss} \end{bmatrix} + B \begin{bmatrix} p_{lv} \\ q_{vad} \\ \end{bmatrix} \tag{3.10}$$

where the output y given as:

$$y = \begin{bmatrix} 1 & 0 & 0 \end{bmatrix} \begin{bmatrix} p_a \\ q_a \\ p_{ss} \end{bmatrix} \tag{3.11}$$

with

$$A = \begin{bmatrix} -\frac{1}{C_a R^*_{av}} & -\frac{1}{C_a} & 0 \\ \frac{1}{L_a} & -\frac{R_a}{L_a} & -\frac{1}{L_a} \\ 0 & \frac{1}{C_s} & -\frac{1}{C_s R_s} \end{bmatrix} \text{ and B} = \begin{bmatrix} \frac{1}{C_a R^*_{av}} & \frac{1}{C_a} \\ 0 & 0 \\ \frac{1}{C_s R_s} & 0 \end{bmatrix} \tag{3.12}$$

If the AoV is closed the AoV resistance can be regarded as infinite. This can be represented by setting entries a_{11} and b_{11} of the state-space model (Equation 3.10) to zero, which results in a linear system. However, in the case that the AoV is opened and the AoV resistance cannot be regarded as infinite. Rüschen et al. (Rüschen et al. (2015)) have shown in a parameter sensitivity analysis, that the AoV resistance has a large influence on the system and should not be represented by a static value. Therefore, the inverse of the AoV resistance is added as a fourth state to the model to allow for a joint parameter and state estimation, thereby making the AoV resistance a varying parameter. However, this results in a non-linear system model, that can be described with the following state-space representation, as represented in Equation 3.14.

The state-vector then becomes:

$$x = \begin{bmatrix} p_a & q_a & p_{ss} & R^{-1}_{av} \end{bmatrix}^T \text{ and the input vector } u = \begin{bmatrix} p_{lv} & q_{vad} \end{bmatrix}^T \tag{3.13}$$

The non-linear state-space model then becomes:

$$\begin{bmatrix} \dot{p}_a \\ \dot{q}_a \\ \dot{p}_{ss} \\ \dot{R}^{-1}_{av} \end{bmatrix} = A \begin{bmatrix} p_a \\ q_a \\ p_{ss} \\ R^{-1}_{av} \end{bmatrix} + B \begin{bmatrix} p_{lv} \\ q_{vad} \\ \end{bmatrix} \tag{3.14}$$

where the output y is

$$y = \begin{bmatrix} 1 & 0 & 0 & 0 \end{bmatrix} \begin{bmatrix} p_a \\ q_a \\ p_{ss} \\ R^{-1}_{av} \end{bmatrix} \tag{3.15}$$

with

$$A = \begin{bmatrix} -\frac{x_4}{C_a} & -\frac{1}{C_a} & 0 & \frac{u_1 - x_1}{C_a} \\ \frac{1}{L_a} & -\frac{R_a}{L_a} & -\frac{1}{L_a} & 0 \\ 0 & \frac{1}{C_s} & -\frac{1}{C_s R_s} & 0 \\ 0 & 0 & 0 & 0 \end{bmatrix} \text{ and B} = \begin{bmatrix} \frac{x_4}{C_a} & \frac{1}{C_a} \\ 0 & 0 \\ \frac{1}{C_s R_s} & 0 \\ 0 & 0 \end{bmatrix} \tag{3.16}$$

The states of the two models are filtered using a KF when the AoV is closed. However, the states are estimated with an EKF when the AoV is determined to be open, due to the non-linearity of the system. The full filtering procedure is described in Appendix A, Figure A.1.

Both filters need predefined covariance matrices that give the filter knowledge on the measurement noise and the process noise. The covariance of the measurement noise, R, has been determined to be 0.34 for the sensors that was used by calculating the mean covariance of a large range of static experiments. The covariance matrices for the process model as proposed by Rüschen et al. (Rüschen et al. (2015)) were also used in our system to allow for good comparison, resulting in the following process covariance matrix for the KF:

$$Q_{KF} = \begin{bmatrix} 7.34 \cdot 10^{-7} & 0 & 0 \\ 0 & 7.1 \cdot 10^{-1} & 0 \\ 0 & 0 & 04.1 \cdot 10^{-3} \end{bmatrix} \tag{3.17}$$

and the covariance matrix for the EKF

$$Q_{EKF} = \begin{bmatrix} 1.92 & 0 & 0 & 0 \\ 0 & 1.2 \cdot 10^{-2} & 0 & 0 \\ 0 & 0 & 04.2 \cdot 10^{-6} & 0 \\ 0 & 0 & 0 & 0 \end{bmatrix} \tag{3.18}$$

When the status of the AoV changes, the estimated states and the covariance matrix are passed from the KF to the EKF or vice versa, in order to assure the consistency of states and covariance throughout the filtering process. As the covariance matrices have a different dimension for both filters, either the fourth state is neglected when the status changes from open to closed or reinitialized with the nominal value when the status changes from closed to open. The error covariance matrix of the state estimate was initialized using an identity matrix. Furthermore, the aortic pressure, p_a, is initialized with the last estimated value of the aortic pressure estimator, the systemic pressure, p_{ss}, with 110 mmHg, the aortic flow, q_a, with the estimated flow through the LVAD and if applicable R_{av}^{-1} with the reciprocal of its nominal value. The system matrices are discretized in each time-step, using a sampling time of $1e^{-3}$.

After processing (S6)

The CO is either obtained from the PF alone or the aortic flow as estimated using the cardiovascular model. This is done by taking a mean average of the respective estimated flow over each heart-cycle (block S6 - Figure 3.3). The cycle is extracted using the range between the occurrence of the SP in two consecutive heart beats and is thus adaptive to changing heart rhythms.

3.3.2 Experiments

In order to evaluate and derive the accuracy of the CO estimator as described in previous section, all experiments that were carried out on the HMC (Section 3.3.1) were used. Using the in vitro data, allowed us to compare the estimated CO with the measured CO.

Therefore, for all six groups of experiments the estimated CO is compared to the measured CO. Firstly, the experiments are conducted using a measurement of the AoV status, thus leaving out the ML model for estimating the AoV status.

Then, as the CO estimator relies on aortic pressure estimator and the PF estimator, the influence of using these estimators in comparison to using measurements of the aortic pressure and PF respectively, was assessed.

Afterwards, the measured AoV status is replaced by the estimation using the ML model and the need for estimating the aortic valve opening status is assessed.

Furthermore, the influence of accurately predicting the opening status of the AoV was evaluated by varying the accuracy of the AoV status prediction between 50% and 100%, thus ranging from random to a perfectly accurate prediction. The error in status prediction was randomized using a uniform random number generator. If the random number was below a certain threshold the AoV status conformed to its actual status. However, when the random number was below a certain threshold, the AoV status was wrong predicted and thus taken as the opposite of its actual status. For example, in case a value of 0.7 was used for the uniform random number generator, then 70% of cycle with open AoV were predicted as open and 70% of the cycles with a closed AoV were predicted as closed, but 30% were predicted as the opposite of the actual status. As ground truth for the prediction, it was determined whether a cycle contained positive measured AoV flows and thus had an AoV opening or contained no such positive flows and thus remained closed.

4 Results

4.1 Ventricular relaxation

Table 4.1 shows the performance of fitting τ_p in sillico for the three selected experiments as summarized in Table 2.1 experiment one, two and three. The first column shows the actual value of τ_2 as predefined in our biexponential model of the left-ventricular elastance. Column two represents the fitted values of τ_p during rest, thus without any changes to the system. Column four and five show τ_p for a preload and afterload increase respectively, which results in an error between 11% and 5% for the first and last experiment respectively. From the first to the second experiment, the relaxation condition changed from $\tau_2 = 0.024$ to $\tau_2 = 0.034$, which is a change of +40%. The 11% inaccuracy in τ_p as observed after an afterload variation in the first experiment is below this 40%. The same holds true for the other experiments. τ_p therefore is able to represent a change in relaxation and shows to be both pre- and afterload independent in the in sillico environment.

Furthermore, the effect of changes in pump-speed on τ_p was assessed in Figure 4.1. Pump-speeds from 3250 to 4500 rpm lead to a maximum range of 0.05 to 0.052 of τ_p, for the experiment with τ_2 is 0.051 (purple line). This is within an absolute range of approximately 2% of the τ_2 value. The effect of pump-speed

Table 4.1: This table shows the estimation of τ_p in seconds at rest and with a preload variation or afterload variation for different time-constants τ_2 of the elastance function.

Experiment	τ_2 (s)	rest	preload variation	afterload variation
1	0.024	0.022	0.0213	0.0213
2	0.034	0.0344	0.0325	0.0321
3	0.43	0.0442	0.420	0.0413
4	0.051	0.0523	0.0499	0.0491
5	0.06	0.0607	0.0584	0.0576
6	0.063	0.0633	0.0611	0.0604

on τ_p in the in sillico environment can thus be neglected.

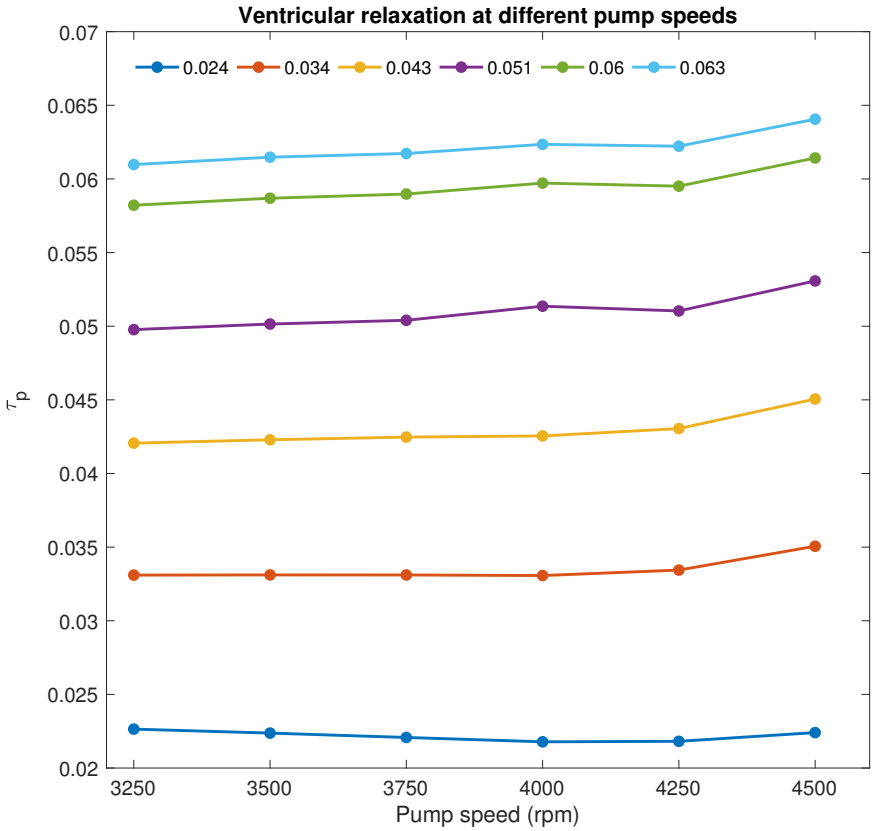

Figure 4.1: This figure shows the effect of changing pump-speed on the time-constant of left-ventricular pressure decay, τ_p, for different relaxation conditions.

The evaluation of τ_p with using the EDPVR as the ground truth did not obtain desirable results. No clear uniformity could be observed between the derived values for τ_p and the respective EDPVR at different stages during the experiments and for all animals. Possible explanations will be covered in the discussion of this thesis (Chapter 5).

4.2 Contractility

Figure 4.2 shows dP/dt_{max} versus EDP for the three experiments that were carried out in sillico starting at the defined baseline pathological levels of contractility, that are 10%, 20%, 30% and 40%. The red dots represent the experiment in which the pre-load is increased. The blue dots show the results of a decrease in after-load. The third experiment, depicted in yellow, shows an increase of 40% in contractility, with steps of 10%, starting from each baseline pathological contractility. It can be clearly observed that changes in contractility result in a much larger effect on dP/dt_{max} versus EDP then the application of a pre-load or afterload change. By applying a pre- or afterload change to the system, dP/dt_{max} versus EDP remains on the same virtual line with respect to the origin. However, applying a contractility change, results in deviation of dP/dt_{max} versus EDP from this virtual line. Therefore, as expected, dP/dt_{max} versus EDP, shows to be a relatively load-independent index of contractility.

Figure 4.3 depicts experiments of increasing preload by 25% over the timespan of the experiment. It can be observed that a change in contractility leads to change in dP/dt_{max} versus EDP, whereas changing the pre-load almost has no effect. A 10% change in contractility has a larger effect than a 25% change in preload.

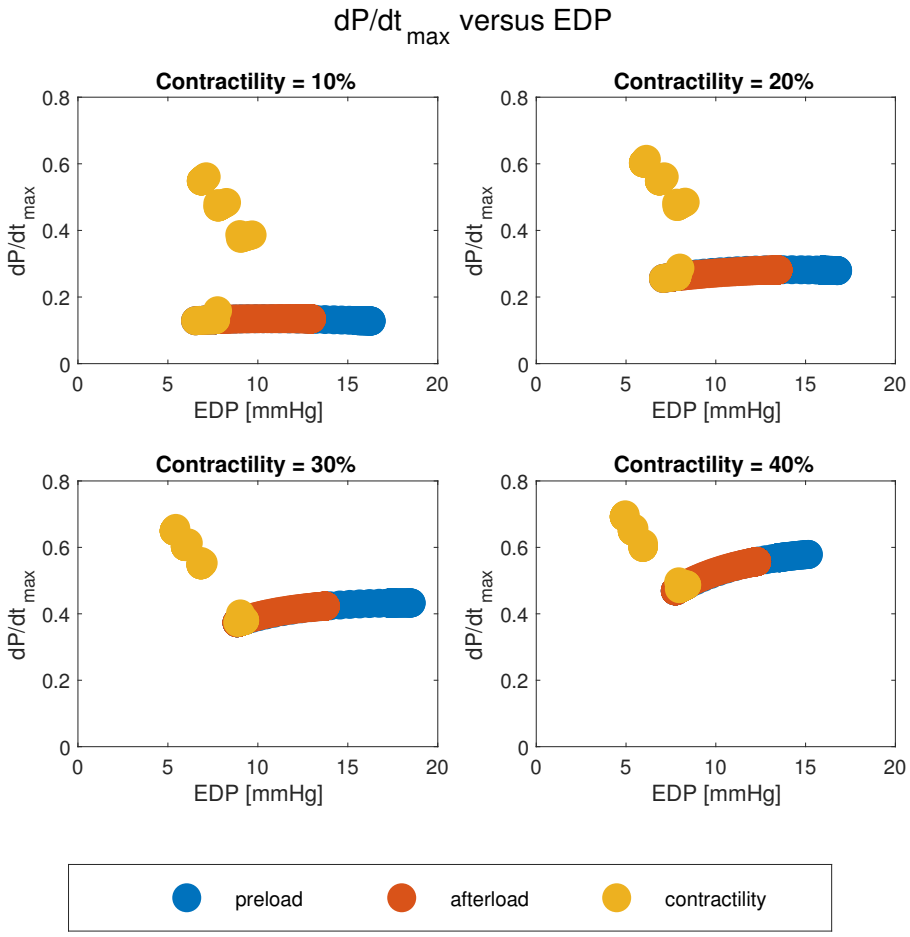

Figure 4.2: The maximum derivative of left-ventricular pressure (dP/dt_{max}) versus the end-diastolic pressure (EDP) at different starting levels of contractility. The blue, red and yellow dots, represent a preload, afterload and contractility variation respectively.

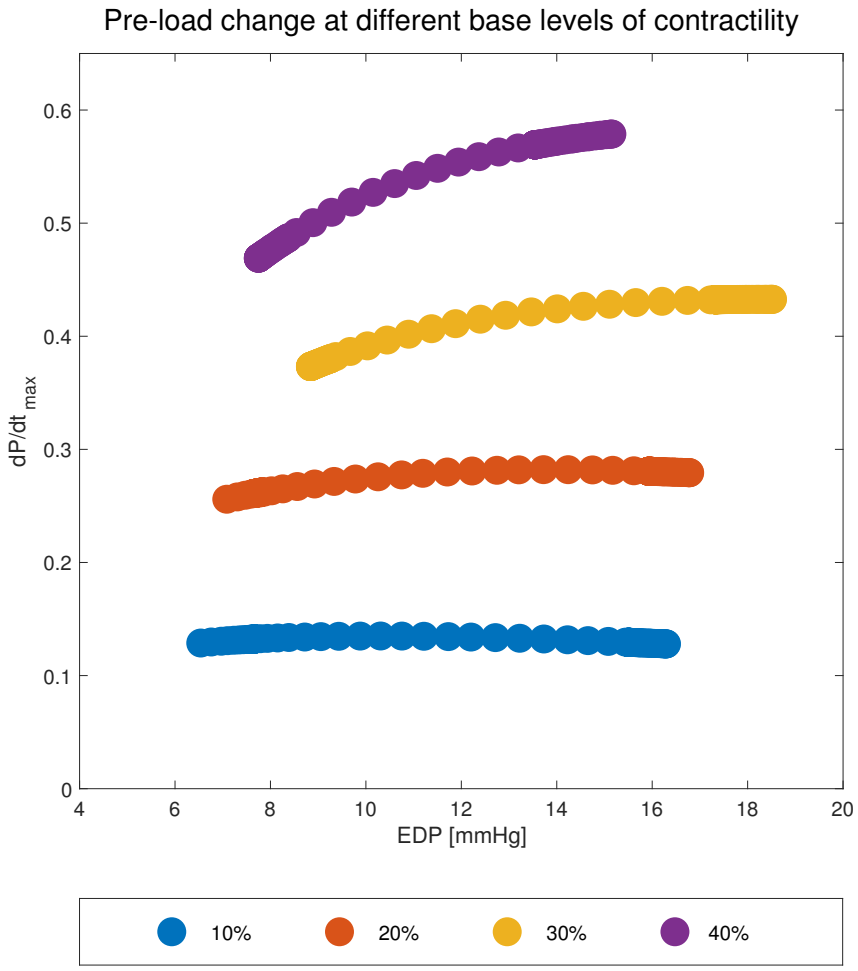

Figure 4.3: The maximum derivative of left-ventricular pressure (dP/dt_{max})) versus the end-diastolic pressure (EDP) after a preload variation at different starting levels of contractility.

For evaluation dP/dt_{max} versus EDP in vivo, two experiments in which adrenaline was infused to the animal at a certain point in time were used. Figure 4.4 depict the relation of dP/dt_{max} versus EDP, where blue is the control data and red data after adrenalin infusion for two different pigs. It is shown that altering the contractile state of the heart by means of adrenalin infusion is reflected in a change in the contractility index. Once steady-state is reached no further rise or fall in the index is observed.

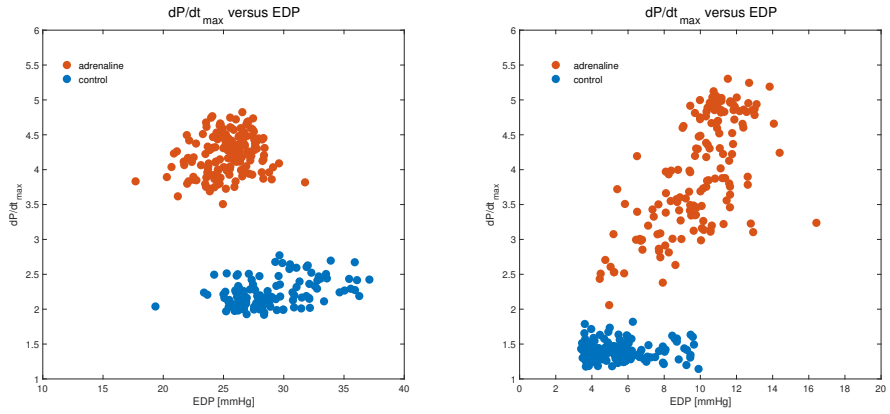

Figure 4.4: The maximum derivative of left-ventricular pressure ,dP/dt_{max}, versus end-diastolic pressure (EDP) with adrenaline infusion for two different pigs

4.3 Cardiac Output

In order to assess the accuracy of the CO estimating scheme, data was gathered from the fifteen experiments that were carried on the HMC, which are summarized in Table 2.2. The experiments were then divided into six groups as described in previous chapter. The cardiac output was then estimated using the monitoring scheme with a measured aortic valve status, thus leaving out the inaccuracy of estimating the state of the aortic valve. As the HMC needs a certain time to reach a steady-state, the first twenty seconds of each experiment were not taken into account. Then the root mean squared error (RMSE) was calculated for all fifteen experiments, after which the average RMSE for the six groups of experiments was calculated. The ground truth for the CO, was determined using a moving average of the measured aortic valve flow and the measured PF over each heart cycle. The RMSE of the estimation of CO compared to the measured CO was assessed (Figure 4.5). Here, the mean of the RMSE was taken for all three control strategies within a group of experiments. For example, the preload variation experiment shows the mean results for continuous pump-speed, physiological control and multi-objective control, whereas the RMSE for the rest experiment is solely based on the continuous pump-speed experiment. Five out of six groups of experiments, exhibit a RMSE of the CO estimation around or below 0.8 L/min.

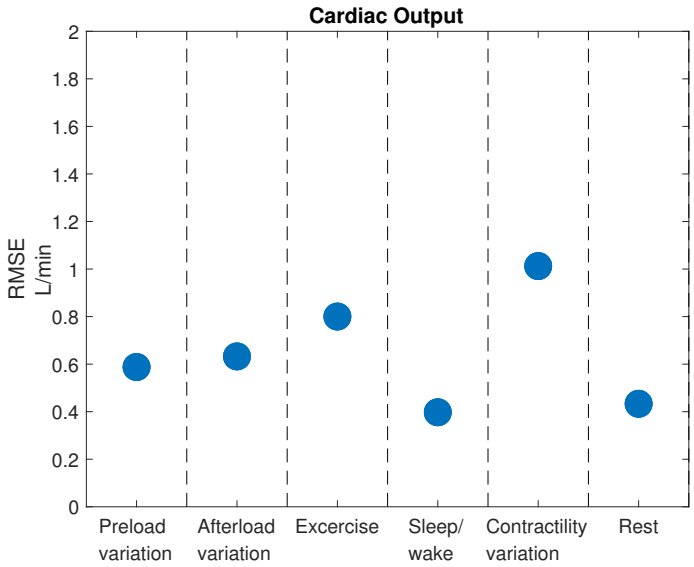

Figure 4.5: This figure shows the root mean squared error (RMSE) between estimated and measured cardiac output (CO) for all experiments in one of the six categories with a measured aortic valve (AoV) opening status.

Table 4.2: This table shows the mean of the measured cardiac output (CO) for the six groups of experiments together with the mean absolute error (MAE) and relative error.

Group	mean (L/min)	MAE (L/min)	error (%)
1	5.1663	0.4683	9.0636
2	4.9873	0.5528	11.0832
3	6.8503	0.6913	10.0911
4	3.8707	0.3457	8.9311
5	4.7915	0.9000	18.7830
6	4.8832	0.3884	7.9547
average	5.0915	0.5577	10.9844

Furthermore, the mean absolute error MAE and the relative error compared to the mean value of the CO were calculated for all experiments as their meaning is easier to interpret compared to the RMSE. The results are depicted in Table 4.2. The relative error of the CO estimation has a maximum of 18% and a minimum of approximately 8%. The average is 11% with a mean absolute error of 0.56 L/min.

The CO estimation relies on the measured LVP and the estimation of the AoP and the PF. Therefore, the influence of using either the PF estimator or the AoP estimator or both compared to their respective measured counterparts on the CO estimation was assessed (Figure 4.6). Using both a measured PF as well as measured AoP results in the highest accuracy of the CO estimation, as can be seen from the blue dots. Furthermore, it can be observed that the PF estimator has a larger influence on the accuracy of the CO estimator than the AoP estimate, which can be seen by comparing the yellow and red dots. In some experiments the CO estimation was more accurate while using the estimated AoP instead of the measured AoP. This was caused by an under estimation of the PF that resulted in an overestimation of the AoP, which led to a larger CO estimation.

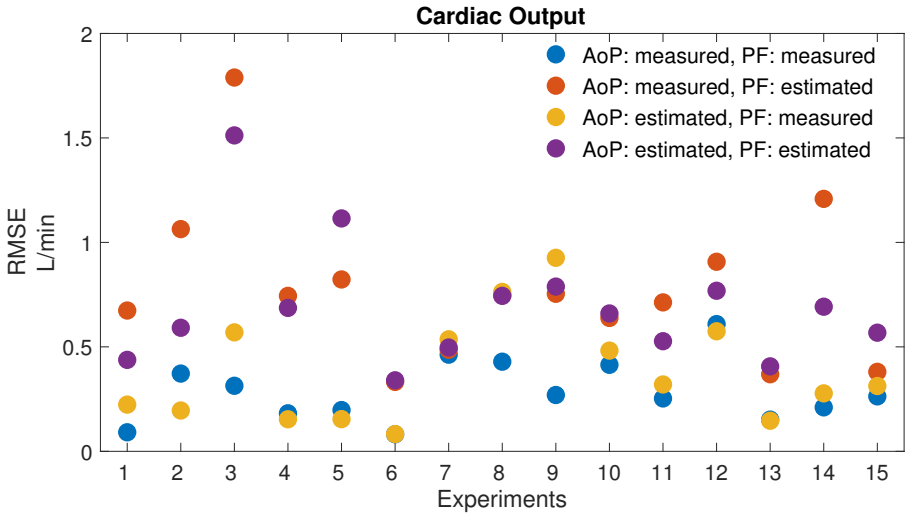

Figure 4.6: This figure shows the influence of using the estimation of the aortic pressure (AoP) and/or pump flow (PF) on the accuracy of the cardiac output (CO) estimation.

Table 4.3: This table shows the mean of the measured AoP for the six groups of experiments together with the mean absolute error (MAE) and relative error.

Group	mean (mmHg)	MAE (mmHg)	error (%)
1	96.0969	9.2443	9.6198
2	86.2734	7.2966	8.4575
3	84.7236	12.0351	14.2052
4	92.0118	6.6252	7.2004
5	94.3320	13.6775	14.4993
6	96.1153	6.2987	10.0893
average	91.5922	9.1962	10.0893

Furthermore, the AoP estimator that contributes to the CO estimation was based on a method that had originally been developed to estimate PF from the pressure head, which is the difference between the AoP and the LVP. However, the AoP estimator in this form is new, which led us to separately assess its performance. Hereto, the AoP estimation was compared to its measured counterpart and the RMSE was calculated for all six groups of experiments as shown in Figure 4.7. The maximum RMSE is 15 mmHg for both the exercise experiments and the contractility variation experiment. The lowest RMSE, 7 mmHg, was observed for the rest experiment, where no variation is applied to the system.

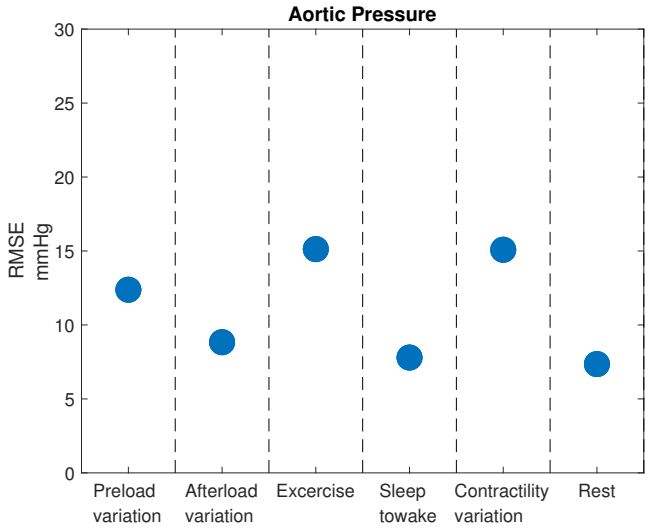

Figure 4.7: This figure shows the root mean squared error (RMSE) between estimated and measured aortic pressure (AoP) for all experiments in one of the six categories.

Moreover, the MAE as well as the relative estimation error compared to the mean value of the aortic pressure for each group of experiments is depicted in Table 4.3. The relative error of the aortic pressure estimation lies in between 7 and 15%.

As the AoP estimation is highly dependent on an accurate PF estimation, the performance of the AoP estimator was assessed at different levels of PF. Hereto, for each of the fifteen experiments, the mean PF throughout the experiment was calculated. Then the RMSE of the estimated AoP was compared for different levels of flow. Higher flows result in larger estimation errors of the AoP (Figure 4.8).

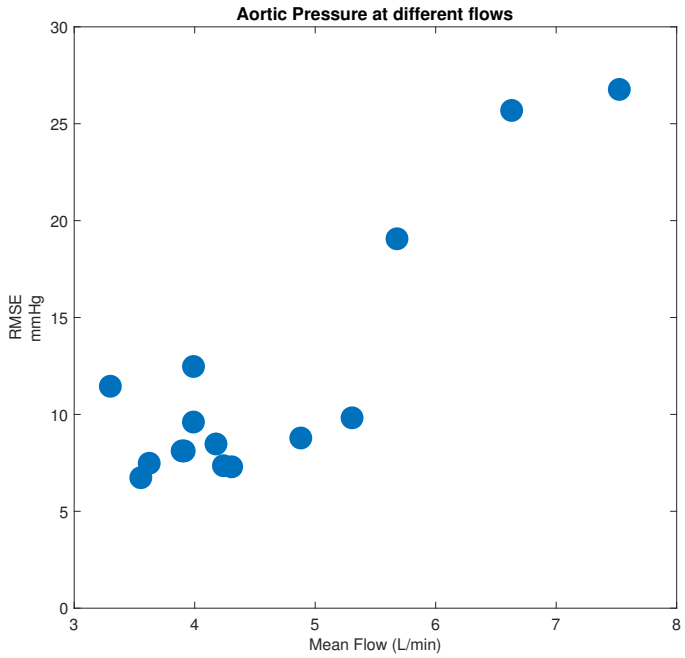

Figure 4.8: This figure shows the root mean squared error (RMSE) between estimated and measured aortic pressure (AoP) for all experiments in one of the six categories, assessed for different levels of pump flow (PF).

The previous results were all derived using the measured aortic valve flow to determine the opening status of the aortic valve. However, as the aortic valve flow is not measurable in patients with LVADs, the machine learning model was implemented to estimate the aortic valve status. In currently implanted LVADs the CO cannot be estimated on line. Therefore, a clinician could use the expected mean of the CO as a guess. A smarter guess of the CO would be to base the expectation on the current activity of the patient. Therefore, for all fifteen experiments in our dataset the mean absolute error MAE was

calculated by using an expected value of 5.09 L/min for the CO, which is the mean CO in our experiments (Table 4.2). This estimation of the CO yielded a MAE of 1.07 L/min. Then the expected CO for each of the six group of experiments was replaced with the mean CO in the respective group (Table 4.2), which resulted in a MAE of 0.93 L/min. Finally, the CO was estimated using the machine learning model for the aortic valve status, resulting in a MAE of 0.86 L/min for all fifteen experiments. Thus, the use of the aortic valve status estimation resulted in a decrease of the MAE of almost 20% compared to using the expected CO. In contrast, using the actual status of the aortic valve, yielded a MAE of 0.56 L/min as depicted in column three of Table 4.2.

The aortic valve status estimator classified 26675 out of 27058 open cycles as such. Closed cycles were determined right 1117 times out of 1493. This resulted in a sensitivity of 0.99 and specificity of 0.7482. This means that the aortic valve status estimator is able to classify cycles with an open valve as such, but works less good for classifying cycles without an aortic valve opening as closed. Furthermore, it can be observed that approximately twenty times as much cycles with an open aortic valve than with a closed aortic valve were present in our dataset. As the two classes of open and closed cycles are not well balanced in the dataset, the Matthews correlation coefficient (MCC) score was calculated. This resulted in a score of 0.73, where one is a perfect prediction and -1 total disagreement. The MCC is regarded to better represent the accuracy of models, whose classes are not balanced.

Moreover, the influence of the accuracy of the AoV status estimator on the CO estimation was assessed. Hereto, the accuracy of predicting cycles with a closed aortic valve as closed and cycles with an open aortic valve as opened was varied, between 50% and 100% (Figure 4.9). Here the purple dots conform to a 100% accurate prediction of the AoV opening status, whereas blue conforms to a 50% accuracy and thus a random guess. Red is 70% accuracy and yellow 90%. The influence ranges from negligible in the case of rest and sleep to wake experiments, to doubling of the RMSE in case of the exercise experiments.

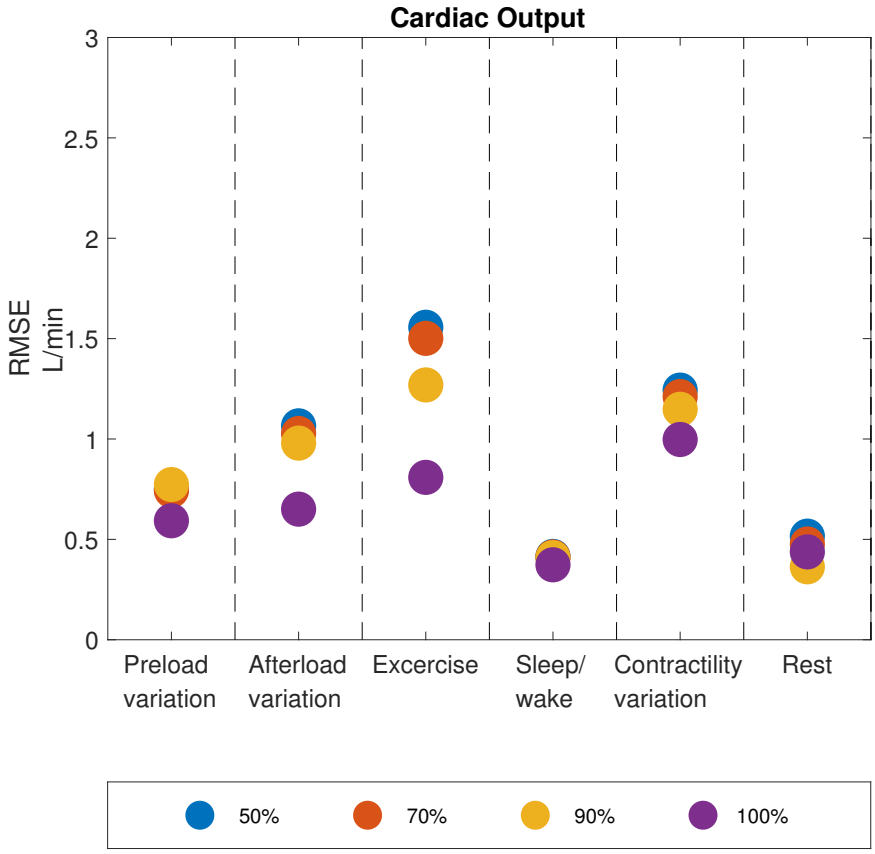

Figure 4.9: The RMSE between estimated and measured cardiac output (CO) for aortic valve (AoV) opening accuracy prediction between 50% and 100% is displayed

The complete system, including the aortic valve opening estimation, was evaluated on all fifteen experiments. The results of the sleep to wake experiment with a physiologic controller and a preload variation at constant speed are described in detail. During the sleep to wake experiment with a physiologic controller, the estimated CO follows the measured CO well. As the PF estimator is able to estimate the actual PF accurately, both the AoP estimator and the CO estimator are not negatively affected. In the first fifty seconds of the experiment, the AoV remains closed. Afterwards, the waking up is simulated as a higher CO is required, which results in an increased pump-speed due to the physiologic controller. The AoV then opens during most cycles and a maximum AoVF of 3 L/min is observed at a PF of 5 L/min.

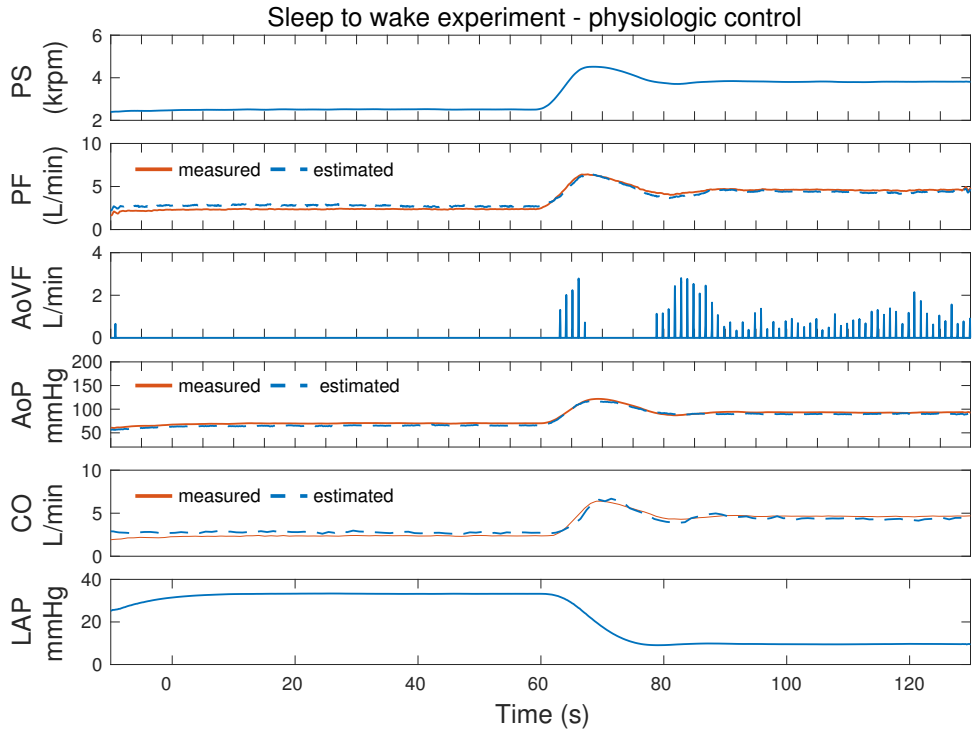

Figure 4.10: Performance results of the cardiac output (CO) estimator with physiological control during a sleep to wake experiment. The signals of pump speed (PS), mean pump flow (PF), cardiac output (CO), , aortic valve flow (AoVF), left atrial pressure (LAP) are depicted.

The CO estimation during a preload variation with a constant pump-speed, shows different results (Figure 4.11). The PF is underestimated throughout the complete experiment. The underestimation of the PF results in an overestimation of the AoP. The CO estimator that relies on the AoP and PF

estimators, when the aortic valve is opened, is not able to estimate the CO as accurate as in the previous experiment. Furthermore, the average AoVF was around 4.42 L/min compared to the sleep to wake experiment (Figure 4.10) which had an average AoVF of 1.7 L/min. In general, it was observed that the CO estimator became less accurate for larger AoVFs.

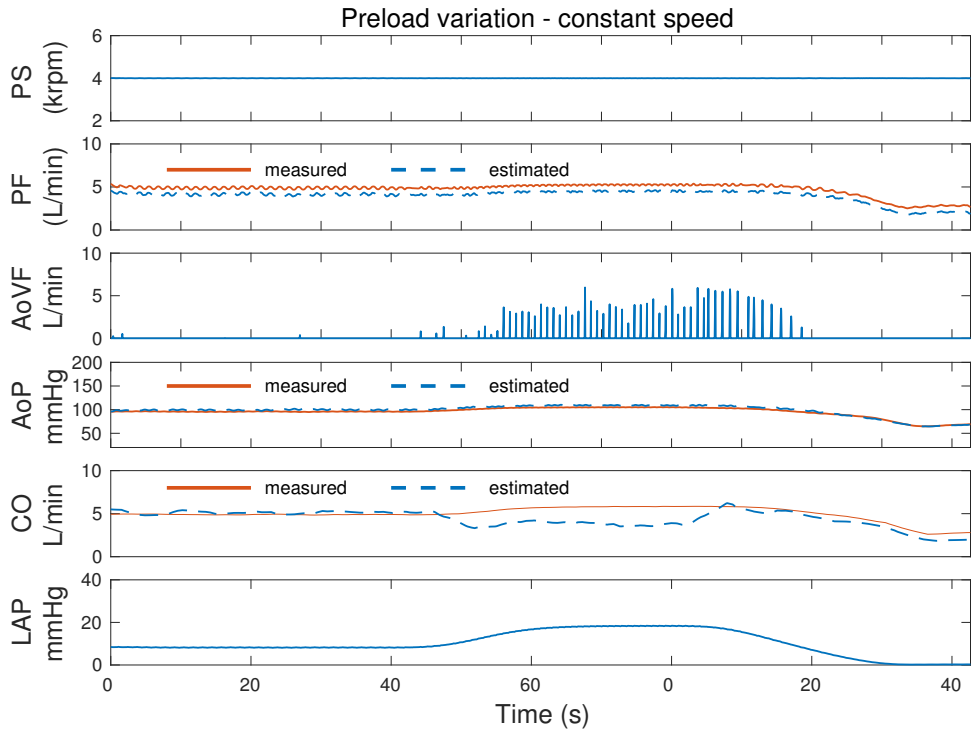

Figure 4.11: Performance results of the cardiac output (CO) estimator with continuous pump-speed during a preload variation. The signals of pump speed (PS), mean pump flow (PF), cardiac output (CO), , aortic valve flow (AoVF), left atrial pressure (LAP) are depicted.

5 Discussion

The goal for this graduation thesis was to develop and test estimators to monitor valuable properties of the heart and circulation under assistance with an LVAD. Hereto, three indices were selected to determine ventricular relaxation, ventricular contractility and the CO. The indices were each evaluated using a different subset of data, ranging from numerical simulations to experiments that were conducted on pigs.

Firstly, the in-vivo experiments that were used in this thesis, were carried out using healthy animals. The added value of using data from real living beings, which allows for incorporating unmodeled dynamics, disturbances and the complex feedback systems of the cardiovascular system, is believed to outweigh the discrepancy between a healthy and unhealthy circulation. However, diseased hearts do exhibit different properties than healthy hearts and thus care should be taken with the interpretation of any result based on the acquired in-vivo data, yet the combination of the in-vivo data with experiments from validated numerical environments of the cardiovascular system, that do allow for simulation of a diseased heart, is promising.

Furthermore, the ventricular relaxation index, τ_p, which had previously been broadly investigated in unassisted hearts, was applied to the circulation with LVAD assistance. The evaluation of the index with numerical simulation data was performed by modeling the left-ventricular elastance, using a bi-exponential function, leading to a mono-exponential decay during diastole, making it possible to model relaxation by means of a changing time-constant. Although, the diastolic part of the left-ventricular does resemble exponential decay in humans, the true form is more complicated and is not influenced solely by left-ventricular relaxation properties of the heart. The exact waveform is not well understood, and a fully comprehensive model does not exist. Although, the results have to be interpreted carefully, the exponential function is believed to be an accurate estimation. Furthermore, it was attempted to show a relation between the EDPVR and τ_p in animal data, where the EDPVR was assumed as the ground truth. The fact that the EDPVR differed in between experiments does not mean that the actual physical properties of

the heart have changed, which is instead highly unlikely to occur over the course of such experiments. Therefore, the relation of τ_p and the EDPVR can only be used to prove the validity of τ_p in real hearts, but not to refute the relation.

Moreover, the contractility index was evaluated using in-vivo experiments, in which the contractile state of the heart was changed by means of adrenaline infusion. The structural properties of the heart are likely to have remained unchanged during the animal trials, but the contractile properties are assumed to have changed due to the adrenaline. However, in diseased hearts the contractility is often influenced by structural properties of the heart. Although, the observed change in the contractility was induced by a pharmacological agent, rather than structural changes that caused the inotropic change, both causes are believed to have the same effect on the contractility index arguing in favor of extrapolating the applicability of the outcomes to diseased hearts.

To estimate the CO, a hybrid system, including both a KF and EKF that were used for filtering the state of the simplified cardiovascular model. It might be possible that this is not be the optimal choice as more complex methods such as a particle filter exist that can be more robust, more accurate and can render the use of a hybrid system unnecessary. However, as for the CO estimation, the mean error over a period of time is more important than the accuracy of each sample in a heart-cycle, the use of an EKF is considered sufficient. Furthermore, the implementation of an EKF is computationally inexpensive and therefore allows for easy online implementation. Also, the choice of an EKF allows for comparison with previous studies, such as the one that was performed by Rüschen et al. (Rüschen et al. (2017)). It was shown that on average a 11% relative error was achieved with respect to the mean CO of the experiments. The mean of mean absolute error over all experiments was 0.55 L/min. In contrast, Rüschen et al. (Rüschen et al. (2017)) have shown a RMSE of 0.16 L/min for an experiment on their HMC, which is similar to the rest experiment, using a constant pump-speed, with a measured AoP and measured PF as seen in Figure 4.6 experiment one. However, the use of multiple control strategies and hemodynamic changes in combination with the use of both an estimated PF and AoP, leads to a deterioration of the estimation. Especially, the PF estimator that was use is known to result in an underestimation at high flows. The performance varies for different flow-levels. Furthermore, the PF is very dependent on the level of support. Therefore, the CO estimation is influenced differently by the PF estimation for different levels of support. In contrast, the aortic pressure is more stable during heart cycles and at different levels of support, hence the possible difference in influence of the CO estimation. The underestimation of the PF at high flows results in higher estimate for the AoP which sometimes partially reduces the underestimation of the total CO estimation.

Furthermore, the average MAE over all fifteen in-vitro experiments for the CO estimation was 0.56 L/min if the AoV status was measured, compared to a MAE of 0.86 in case the ML model was used. Besides the estimation error due the cycles that were unjustly classified as either open or closed, another problem was observed during evaluation. If the AoV was classified as open, the occurrence of the AoV opening was sometimes estimated to take place before the actual opening. Also, the duration of the AoV opening often differed from the actual duration of the valve opening. Especially, the period during the cycle at which the AoV is determined to be opened, is of key importance. Deviations from the actual AoV opening period may result in estimation errors as CO estimator used values of PF and AoP that differ from values that are usually observed during the AoV opening. Although, this issue affected the CO estimation, still good results were obtained, stressing the robustness of the estimator.

6 Conclusion

The goal of this thesis was to develop and evaluate three indices to monitor cardiac properties in a circulation with left-ventricular assistance.

With respect of the measure for ventricular relaxation, τ_p, we were able to implement the method in our testing environment using a biexponential elastance function as proposed by Sun et al. Sun (1991). It has then been shown that τ_p is able to capture changes in this elastance function that is directly related to the relaxation properties of the heart. The measure τ_p has been shown to be both preload and afterload independent and to be minimally affected by changes of pump-speed within the operating range of the LVAD. Unfortunately, we were not able to prove the validity and accuracy of τ_p in pigs. The experiments that were had to our disposal did not incorporate an induced change of relaxation while keeping all factors equal, making it impossible to determine a ground truth in these experiments. However, the applicability of τ_p in simulations on the validated cardiovascular model, together with the understanding that the decaying part of the left-ventricular pressure resembles exponential decay in animals as well as humans, leads us to believe that the method might be used in the clinical setting.

The contractility index dP/dt_{max} versus EDP was evaluated using both experiments on the HMC as well as data from the acute animal trials. dP/dt_{max} versus EDP showed to be both preload and afterload dependent, but more importantly captured the effect of applied contractility changes starting from different base levels of disease in simulation data. Also, changing the contractile state in healthy pigs, was reflected in a change of the contractility index in the same direction. Therefore, dP/dt_{max} versus EDP, has shown to be a valuable indicator of contractility in the in sillico as well as in vivo setting. The implementation of this index in clinically used LVAD, might lead to a better understanding of progression of disease in heart patients with left-ventricular assistance.

Also, the CO is an important physiological parameter during LVAD therapy as it gives insight in the level of systemic perfusion and therefore the delivery

of oxygenated blood to the organs. The CO was estimated using a hybrid monitoring scheme and was thoroughly evaluated on data from the HMC using six groups of experiments. The results of the estimation of the CO by solely making use of the PIP and pump-intrinsic signals has shown to be very promising and leads to errors within the clinically accepted bounds.

In conclusion, the goal of this thesis was to explore the possibilities of the PIP sensor for acquiring valuable information of the state of the heart. It was possible to accurately determine both contractility and relaxation properties of the heart in simulated experiments, independent of common hemodynamic changes such as preload and afterload variation. Moreover, it was shown that the contractility index reflected contractility changes in animal data. Last, the possibility of accurately estimating the CO, solely based on the pump-intrinsic signals in combination with the PIP, was demonstrated.

The online implementation of the proposed estimators for left-ventricular relaxation, cardiac contractility and the CO in the clinical setting can provide clinicians with valuable and reliable information of the circulation of the patient, allowing for monitoring of progression of disease and the improvement of treatment. This can result in a better quality of life.

7 Recommendations

Before the proposed and evaluated estimators can be implemented in the clinical setting, it is recommended to further ensure the robustness and improve their accuracy in various experiments. Unfortunately, the validity of using τ_p as a measure of ventricular relaxation could not be verified with the accessible animal data. Therefore, it is suggested that future research should focus on testing this index in ex vivo trials with human or animal hearts of which the relaxation properties can be inferred.

The contractility index has shown to be an accurate estimator and is able to reflect inotropic changes in both in vitro as well as in vivo data. As the sensitivity to contractile changes in pigs was inferred from two experiments in which the contractility was influenced by adrenaline, more controlled experiments have to be performed. The use of hearts that of which the physical properties are affected by disease, rather than by the use of inotropic agents such as adrenaline is recommended. This can be done with ex vivo trials with human or animal heats, but also possibly in chronic animal trials where the physical properties of the heart can be affected.

Last, the CO estimation based on the pump-intrinsic signals as well as the PIP has shown promising results on in vitro experiments that were obtained with the HMC. Before implementation in clinically used LVADs, the experiments should be repeated in animal trials. Furthermore, the estimation of the duration of the AoV opening within a cycle as well as the AoV opening status estimator should be improved. Also, models that better represent the system of interest may developed and examined which can result in an improved estimation of the CO. Last, the use of estimators, for estimating the states of such models, which may be more robust in non-linear systems or that can eliminate the need of using a hybrid system, such as particle filters could become a direction of research.

A Appendix

A.1 Extended Kalman filter

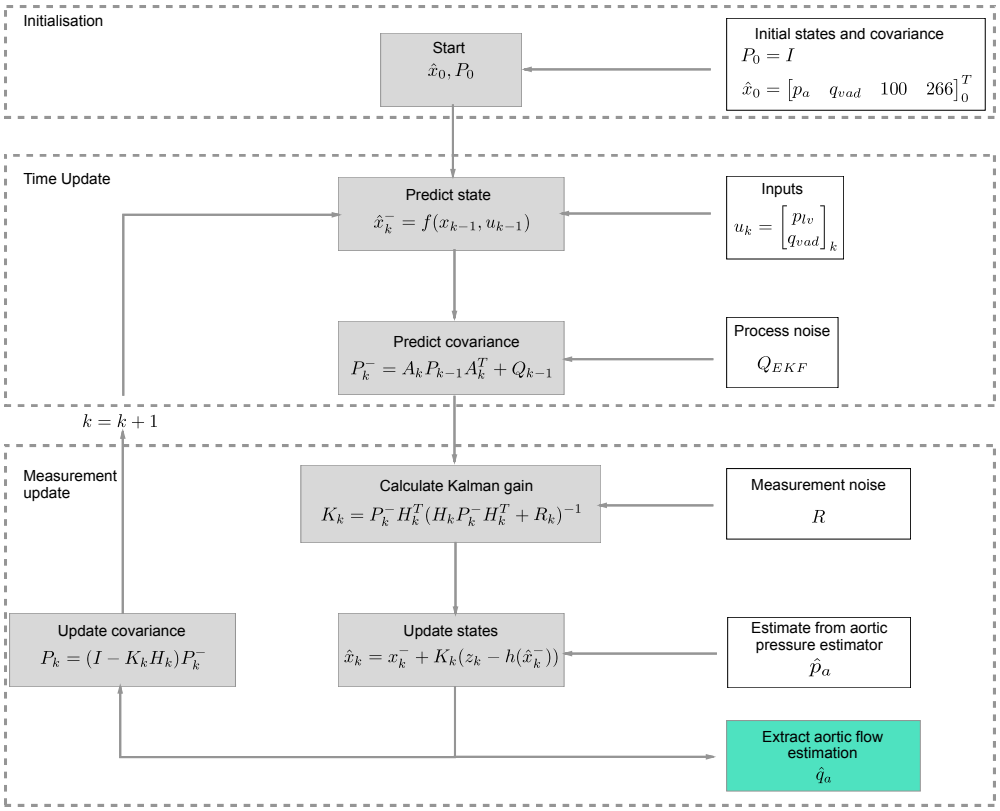

Figure A.1: Schematic of the Extended Kalman Filter (EKF). The aortic flow is estimated and extracted at each time-step and is then further processed to obtain the cardiac output (CO).

A.2 In vitro experiments

Table A.1: This table shows fifteen experiments that were performed on the hybrid mock circulation (HMC). Here CS is constant-speed, MOC is multi-objective control and PC is physiological control.

Exp	Dscription	Controller
1	Rest	CS
2	Contractility variation	CS
3	Exercise	CS
4	Sleep to wake	CS
5	Preload variation	CS
6	Afterload variation	CS
7	Preload variation	MOC
8	Afterload variation	MOC
9	Exercise	MOC
10	Contractility variation	MOC
11	Preload variation	PC
12	Afterload variation	PC
13	Exercise	PC
14	Sleep to wake	PC
15	Contractility variation	PC

B Source Code

Code B.1: Source Code for biexponential elastance

```
function [p] = BiexponentialTimeVaryingElastance(
   Volume,phase,tau_in)


% naming constants
T1 = 0.8333;          % [%/100]
T2 = 0.5;             % [%/100]
V_pmax = 200;         % [ml]
P_max = 25;           % [mmHg]
Emin = 0.1;           % [mmHg/ml]
K = 0;                % [-]
V_sat = 221.4;        % [ml]
P_0 = 0;              % [mmHg]
V_0 = 14.6;           % [ml]
Ri_min = 0;           % [mmHg*s/ml]
Ri_max = 0.03;        % [mmHg*s/ml]


%naming constants biexponential function
E_lva = 3;            %c scaling parameter
E_lvb = 0.05;         %c scaling parameter
tau_1 = 0.3;          %ms
tau_2 = tau_in;       %ms
t_ee  = 0.4165;       %ms
t_tau   = 0.833;      %ms

P11 = 2*pi*t_ee;
P22 = 2*pi*t_tau;
```

```
persistent e_lv_max
if isempty(e_lv_max)
    e_lv_max = 1;
end

% Ventricular biexponential contraction function:
   e_lv (Sun et al. 1991)
if phase <= P11
    e_lv = E_lva*(1-exp(-(phase/2/pi)/tau_1)) +
       E_lvb;
    e_lv_max = max(e_lv_max, e_lv);
elseif phase <= P22
    e_lv_t_ee = e_lv_max;
    e_lv = (e_lv_t_ee-E_lvb)*exp(-((phase/2/pi)-t_ee
       )/tau_2) + E_lvb;
else
    e_lv = 0;
end

e_lv = e_lv/e_lv_max;

% End-systolic pressure-volume relation (ESPVR)
phi_a = (1 - ((V_pmax - V)/(V_pmax - V_0))^2 )*P_max
   ;

% End-diastolic pressure-volume relation (EDPVR)
phi_p = Emin*(V - V_0) + K /(V_sat - (V - V_0)) - K/
   V_sat;

d_phi = phi_a - phi_p;
if d_phi < 0
    d_phi = 0;
end

% Instantaneous ventricular pressure
phi = phi_p + d_phi*e_lv;
p = P_0 + phi;
```

List of Figures

List of Tables

List of Codes

Bibliography

Colacino, F. M., Moscato, F., Piedimonte, F., Arabia, M. & Danieli, G. A. (2007), 'Left ventricle load impedance control by apical VAD can help heart recovery and patient perfusion: a numerical study.', *ASAIO journal (American Society for Artificial Internal Organs : 1992)* **53**(3), 263--277.

Davis, J., Sanford, D., Schilling, J., Hardi, A. & Colditz, G. (2015), 'Systematic review of outcomes after noncardiac surgery in patients with implanted left ventricular assist devices', *ASAIO Journal* **61**(6), 648--651.

Dunlay, S. M., Strand, J. J., Wordingham, S. E., Stulak, J. M., Luckhardt, A. J. & Swetz, K. M. (2016), 'Dying with a Left Ventricular Assist Device as Destination Therapy', *Circulation: Heart Failure* **9**(10), 1--9.

Granegger, M., Moscato, F., Casas, F., Wieselthaler, G. & Schima, H. (2012), 'Development of a pump flow estimator for rotary blood pumps to enhance monitoring of ventricular function', *Artificial Organs* **36**(8), 691--699.

Kasner, M., Westermann, D., Steendijk, P., Gaub, R., Wilkenshoff, U., Weitmann, K., Hoffmann, W., Poller, W., Schultheiss, H. P., Pauschinger, M. & Tschöpe, C. (2007), 'Utility of Doppler echocardiography and tissue Doppler imaging in the estimation of diastolic function in heart failure with normal ejection fraction: A comparative Doppler-conductance catheterization study', *Circulation* **116**(6), 637--647.

Mason, D. T., Braunwald, E., Covell, J. W., Sonnenblick, E. H. & Ross, J. (1971), 'Assessment of cardiac contractility. The relation between the rate of pressure rise and ventricular pressure during isovolumic systole.', *Circulation* **44**(1), 47--58.

Moscato, F., Danieli, G. A. & Schima, H. (2009), 'Dynamic modeling and identification of an axial flow ventricular assist device.', *The International journal of artificial organs* **32**(6), 336--43.

Moscato, F., Granegger, M., Naiyanetr, P., Wieselthaler, G. & Schima, H. (2012), 'Evaluation of Left Ventricular Relaxation in Rotary Blood

Pump Recipients Using the Pump Flow Waveform: A Simulation Study', *Artificial Organs* **36**(5), 470--478.

Ochsner, G., Amacher, R., Amstutz, A., Plass, A., Daners, M. S., Tevaearai, H., Vandenberghe, S., Wilhelm, M. J. & Guzzella, L. (2013), 'A novel interface for hybrid mock circulations to evaluate ventricular assist devices', *IEEE Transactions on Biomedical Engineering* **60**(2), 507--516.

Ochsner, G., Amacher, R., Wilhelm, M. J., Vandenberghe, S., Tevaearai, H., Plass, A., Amstutz, A., Falk, V. & Schmid Daners, M. (2014), 'A Physiological Controller for Turbodynamic Ventricular Assist Devices Based on a Measurement of the Left Ventricular Volume', *Artificial Organs* **38**(7), 527--538.

Ochsner, G., Wilhelm, M. J., Amacher, R., Petrou, A., Cesarovic, N., Staufert, S., Röhrnbauer, B., Maisano, F., Hierold, C., Meboldt, M. & Daners, M. S. (2017), 'In Vivo Evaluation of Physiologic Control Algorithms for Left Ventricular Assist Devices Based on Left Ventricular Volume or Pressure', *ASAIO Journal* **63**(5), 568--577.

Paulus, W. J., Tschöpe, C., Sanderson, J. E., Rusconi, C., Flachskampf, F. a., Rademakers, F. E., Marino, P., Smiseth, O. a., De Keulenaer, G., Leite-Moreira, A. F., Borbély, A., Edes, I., Handoko, M. L., Heymans, S., Pezzali, N., Pieske, B., Dickstein, K., Fraser, A. G. & Brutsaert, D. L. (2007), 'How to diagnose diastolic heart failure: a consensus statement on the diagnosis of heart failure with normal left ventricular ejection fraction', *European heart journal* **28**(20), 2539--50.

Petrou, A., Lee, J., Dual, S., Ochsner, G., Meboldt, M. & Schmid Daners, M. (2018), 'Standardized Comparison of Selected Physiological Controllers for Rotary Blood Pumps: In Vitro Study', *Artificial Organs* **42**(3), E29--E42.

Petrou, A., Monn, M., Meboldt, M. & Schmid Daners, M. (2017), 'A Novel Multi-objective Physiological Control System for Rotary Left Ventricular Assist Devices', *Annals of Biomedical Engineering* **45**(12), 2899--2910.

Petrou, A., Ochsner, G., Amacher, R., Pergantis, P., Rebholz, M., Meboldt, M., Daners, M. S. & Schmid Daners, M. (2016), 'A Physiological Controller for Turbodynamic Ventricular Assist Devices Based on Left Ventricular Systolic Pressure', *Artificial Organs* **40**(7), 842--855.

Ponikowski, P., Voors, A. A., Anker, S. D., Bueno, H., Cleland, J. G., Coats, A. J., Falk, V., González-Juanatey, J. R., Harjola, V. P., Jankowska, E. A., Jessup, M., Linde, C., Nihoyannopoulos, P., Parissis, J. T., Pieske, B., Riley, J. P., Rosano, G. M., Ruilope, L. M., Ruschitzka, F., Rutten, F. H.

& Van Der Meer, P. (2016), '2016 ESC Guidelines for the diagnosis and treatment of acute and chronic heart failure', *European Heart Journal* **37**(27), 2129--2200m.

Riebandt, J., Haberl, T., Mahr, S., Laufer, G., Rajek, A., Steinlechner, B., Schima, H. & Zimpfer, D. (2014), 'Preoperative patient optimization using extracorporeal life support improves outcomes of INTERMACS Level I patients receiving a permanent ventricular assist device', *European Journal of Cardio-thoracic Surgery* **46**(3), 486--492.

Rüschen, D., Prochazka, F., Amacher, R., Bergmann, L., Leonhardt, S. & Walter, M. (2017), 'Biomedical Signal Processing and Control Minimizing left ventricular stroke work with iterative learning flow profile control of rotary blood pumps', *Biomedical Signal Processing and Control* **31**, 444--451.

Rüschen, D., Rimke, M., Gesenhues, J., Leonhardt, S. & Walter, M. (2015), 'Online cardiac output estimation during transvalvular left ventricular assistance', *Computer Methods and Programs in Biomedicine* .

Simaan, M. A., Ferreira, A., Member, S., Chen, S., Antaki, J. F. & Galati, D. G. (2009), 'A Dynamical State Space Representation and Performance Analysis of a Feedback-Controlled Rotary Left Ventricular Assist Device', *IEEE Transactions on Control Systems Technology* **17**(1), 15--28.

Sun, Y. (1991), 'Modeling the dynamic interaction between left ventricle and intra-aortic balloon pump.', *The American journal of physiology* **261**(4 Pt 2), H1300--11.

Van Riet, E. E., Hoes, A. W., Wagenaar, K. P., Limburg, A., Landman, M. A. & Rutten, F. H. (2016), 'Epidemiology of heart failure: The prevalence of heart failure and ventricular dysfunction in older adults over time. A systematic review', *European Journal of Heart Failure* **18**(3), 242--252.

Weiss, J. L., Frederiksen, J. W. & Weisfeldt, M. L. (1976), 'Hemodynamic determinants of the time-course of fall in canine left ventricular pressure.', *Journal of Clinical Investigation* **58**(3), 751--760.

Zile, M. R. (2002), 'New Concepts in Diastolic Dysfunction and Diastolic Heart Failure: Part I: Diagnosis, Prognosis, and Measurements of Diastolic Function', *Circulation* **105**, 1387--1393.